

Nonpeptide Urotensin-II Receptor Antagonists: A New Ligand Class Based on Piperazino-Phthalimide and Piperazino-Isoindolinone Subunits

Edward C. Lawson,* Diane K. Luci, Shyamali Ghosh, William A. Kinney, Charles H. Reynolds, Jenson Qi, Charles E. Smith, Yuanping Wang, Lisa K. Minor, Barbara J. Haertlein, Tom J. Parry, Bruce P. Damiano, and Bruce E. Maryanoff*

Johnson & Johnson Pharmaceutical Research & Development, Welsh & McKean Roads, Spring House, Pennsylvania 19477-0776

Received May 21, 2009

We have discovered two related chemical series of nonpeptide urotensin-II (U-II) receptor antagonists based on piperazino-phthalimide (**5** and **6**) and piperazino-isoindolinone (**7**) scaffolds. These structure types are distinctive from those of U-II receptor antagonist series reported in the literature. Antagonist **7a** exhibited single-digit nanomolar potency in rat and human cell-based functional assays, as well as strong binding to the human U-II receptor. In advanced pharmacological testing, **7a** blocked the effects of U-II in vitro in a rat aortic ring assay and in vivo in a rat ear-flush model. A discussion of U-II receptor antagonist pharmacophores is presented, and a specifically defined model is suggested from tricycle **13**, which has a high degree of conformational constraint.

Introduction

The cyclic peptide urotensin-II (U-II^a) activates the urotensin-II receptor (UT), a G-protein-coupled receptor that was originally identified as “orphan” receptor GPR14,¹ and is expressed in many tissues, including blood vessels, heart, liver, kidney, skeletal muscle, and lung.² Actually, there is a collection of U-II peptides that range in size from 11 to 14 amino acids across species, from fish to humans, with 11 amino acids in humans to 14 amino acids in mice. Residues 5 through 10 of these U-II peptides comprise a highly conserved CFWKYC cyclic array, whereas the N-terminal region is variable in length and constitution. The WKY motif has been identified as being important for biological activity.³

U-II from the urophys of the goby fish (*Gillichthys mirabilis*) is a 12-mer cyclic peptide that may well be the most potent vasoconstrictor known.^{4–6} This compound caused concentration-dependent contraction of isolated arterial rings of rats and humans with an EC₅₀ less than 1 nM. However, the in vivo effects of U-II can be contradictory because of varied specificity for different tissues and different species. As a case in point, U-II was reported to cause vasodilation in conscious rats.⁷ Nevertheless, relative to the role of U-II in chronic vascular disease, the goby U-II peptide induced hypertrophy in cardiomyocytes⁸ and the proliferation of smooth muscle cells,⁹ indicating a potential role in heart

failure and atherosclerosis. From the wealth of knowledge in this area, U-II and its receptor have been implicated in various cardiorenal and metabolic diseases,^{1a–c} including hypertension,¹⁰ heart failure,¹¹ chronic renal failure,^{11c,12} diabetes,^{11c,13} and atherosclerosis.¹⁴ Consequently, we^{3b,15} and other researchers^{3a,3c,16,17} have been pursuing U-II receptor antagonists as potential therapeutic agents.

To obtain initial lead structures, we devised and executed a high-throughput screening (HTS) protocol involving a functional assay based on cells transfected with rat UT, a fluorometric imaging plate reader (FLIPR) to measure intracellular calcium flux, and the potent, cyclopeptide U-II agonist Ac-CFWK(2-Nal)C-NH₂ (**1**; rat FLIPR EC₅₀ = 0.54 nM, rat UT binding K_i = 0.12 nM) (Chart 1; see Experimental Section).^{3b} Application of this assay to a large compound library (~500000 entities) resulted in several confirmed hits, one of which was moderately potent, nonpeptide antagonist **2** (rat FLIPR IC₅₀ = 1 μM) (Chart 1). Unfortunately, this compound and its more potent bis-desfluoro analogue, **3** (rat FLIPR IC₅₀ = 150 nM), turned out to be metabolically unstable to human liver microsomes (HLM *t*_{1/2} < 3 min), primarily because of piperazine debenzoylation (Chart 1). As part of a drug discovery endeavor, we sought to mitigate this metabolic problem and improve U-II receptor antagonist potency. This effort led to a new class of potent UT antagonists based on piperazino-phthalimide and piperazino-isoindolinone structural subunits (Table 1, compounds **2–4**, **5a–n**, **6a–j**; Table 2, compounds **7a–o**). In this paper, we present our results with these novel series and discuss U-II receptor antagonist pharmacophores.

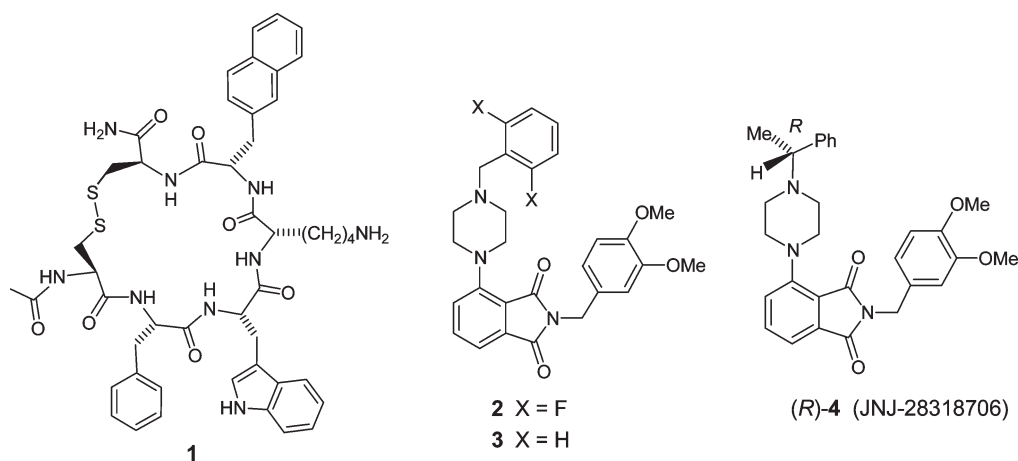
Results and Discussion

Synthetic Chemistry. Prototype phthalimide **3** was prepared by the route outlined in Scheme 1. Hydroxyphthalimide **I** was coupled with veratrylamine in the presence of triethylamine, followed by triflate formation to give **II** in

*To whom correspondence should be addressed. Phone: 215-628-5644 (E.C.L.); 215-628-5530 (B.E.M.). Fax: 215-540-4612. E-mail: elawson@its.jnj.com (E.C.L.); bmaryano@its.jnj.com (B.E.M.).

^a Abbreviations: BOP, benzotriazol-1-yloxy-tris(dimethylamino)-phosphonium; BSA, bovine serum albumin; CHO, Chinese hamster ovary; dba, (*E,E*)-dibenzylideneacetone; FLIPR, fluorometric imaging plate reader; h, human; HBTU, *O*-benzotriazol-1-yl-*N,N,N'*-tetramethyluronium; HOBt, 1-hydroxybenzotriazole; HLM, human liver microsomes; HTS, high-throughput screening; PK, pharmacokinetics; SAR, structure–activity relationship; TFA, trifluoroacetic acid; Tol-BINAP, 2,2'-bis(di-*p*-tolyl)phosphino-1,1'-binaphthyl; U-II, urotensin-II; UT, urotensin-II receptor.

Chart 1



excellent yield. Boc-piperazine was introduced by direct displacement in the presence of triethylamine at 110 °C in a sealed tube in good yield. The Boc group was removed and **III** was alkylated with benzyl bromide to afford **3** in high yield.

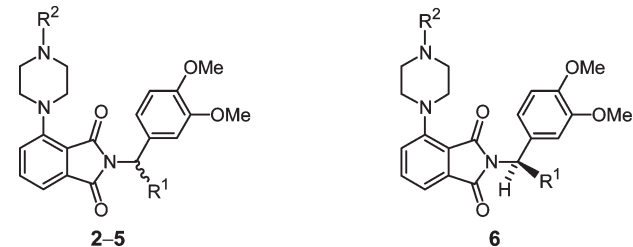
Compounds of structure type **5** were prepared according to the general plan in Scheme 2. Ketones **V** were obtained from carboxylic acids **IV** by Weinreb amide formation, followed by addition of 3,4-dimethoxyphenylmagnesium bromide.¹⁸ Reductive amination with ammonium acetate and sodium cyanoborohydride gave primary benzylamines **VI**, which were converted into phthalimides **VII**. Activation as a triflate and piperazine displacement yielded target piperazino-phthalimides **5** (Table 1). 2-Thienylsulfonamidoalkyl derivatives **5e**, **5g**, and **5j** were prepared from the corresponding primary amines and 2-thienylsulfonfyl chloride with K₂CO₃ as a base. In the case of (*R,S*)-**5a**, an enantioselective synthesis was performed (Scheme 3). Thus, ketone **VIII** was reduced asymmetrically with borane and prolinol **IX**¹⁹ to alcohol **X** in high yield, with an optical rotation of $[\alpha]^{25}_{\text{D}} +42.0$ (*c* 1.07, CHCl₃). Since Ponzio and Kaufman reported an optical rotation for **X** of $[\alpha]^{25}_{\text{D}} +40.5$ (*c* 1.1, CHCl₃), corresponding to 97% ee,¹⁹ our material was considered to be essentially $\geq 99\%$ ee. The mesylate of **X** was reacted with diallylamine to give **XI** in good yield with inversion of the stereocenter. The allyl groups were removed by a palladium catalysis procedure²⁰ and **XII** was transformed into target (*R,S*)-**5a**, $[\alpha]^{25}_{\text{D}} +13.8$ (*c* 1.18, CH₃OH), by generation of a phthalimide, formation of a triflate, and displacement with piperazine **XIII** (8% yield for four steps). On the basis of the chemistry used, (*R,S*)-**5a** should have been $>99\%$ ee.

We developed an enantioselective synthesis of key diamine enantiomers (*R*)-**XVI** and (*S*)-**XVI** to provide individual diastereomers for testing (Scheme 4; exemplified for (*R*)-**XVI**). Weinreb amide **XIV**¹⁶ was subjected to asymmetric reductive amination by using ammonium formate and a chiral Binaphthylruthenium complex to give **XV** (96% ee).²¹ The primary amine in (*R*)-**XV** was protected as a trifluoroacetamide, the Cbz group was removed, a Boc group was installed, and the trifluoroacetyl group was removed to afford (*R*)-**XVI**. The incorporation of this intermediate into a final product is illustrated for **7a** in Scheme 5. Benzoic acid **XVII** was esterified and α -brominated to give **XVIII**, which was coupled with (*R*)-**XVI** and cyclized thermally to indolinone **XIX**. The aryl halide was displaced by *N*-ethylpiperazine

under palladium catalysis to give **XX**.²² The Boc group was removed, and the exposed primary amine was coupled with 2-thienylsulfonfyl chloride to furnish target compound **7a** (96% ee; see Experimental Section).

Development of U-II Receptor Antagonists. As an early approach to metabolic stabilization, we installed an α -methyl group to generate (*R*)-**4** (Chart 1). We realized improved metabolic stability (HLM $t_{1/2}$ = 29 min) and improved potency (rat FLIPR IC₅₀ = 84 nM);²³ also, (*R*)-**4** proved to be promising in that it exhibited good oral bioavailability in a pharmacokinetics (PK) experiment in rats (*F* = 33%, $t_{1/2}$ = 4 h). However, in a whole-cell binding assay involving human UT (see Experimental Section),²⁴ (*R*)-**4** had just moderate affinity (hUT *K*_i = 570 nM). Now, the goal became improvement of binding affinity for the human receptor while retaining favorable rat potency (because rats would serve the pharmacological test species) and metabolic stability. We carried out a structure–activity relationship (SAR) study with respect to the 3,4-dimethoxyphenyl segment and found that the 3,4-dimethoxyphenyl group is crucial for decent in vitro potency. Without going into much detail, the following replacements for 3,4-dimethoxyphenyl in prototype (*R*)-**4** were very unfavorable: phenyl, 3-hydroxy-4-methoxyphenyl, 3-methoxy-4-hydroxyphenyl, 3-ethoxy-4-methoxyphenyl, 3-methoxy-4-ethoxyphenyl, 4-benzoic acid methyl ester, 3-benzoic acid methyl ester, 4-benzoic acid, 3-benzoic acid, 2-pyrimidine, 3-indole, 4-indole, 2-methoxypyridine, and 5,6-dimethoxy-1-indane.

We explored the attachment of substituents onto the methylene portion of the 3,4-dimethoxybenzyl group to probe SAR around that benzylic position. Thus, mono- α -substituted 3,4-dimethoxybenzylamines (**VI**) were converted into phthalimide products **5** (Scheme 2). The rat FLIPR potency of methyl derivative **5a** (IC₅₀ = 70 nM) was in the range of unsubstituted compound **4** (Table 1). Diastereomer (*R,S*)-**5a** had a rat FLIPR IC₅₀ value of 130 nM, as well as a 3.5-fold potency improvement for the human receptor (hUT *K*_i = 160 nM) compared to **4**.²⁵ Ethyl analogue **5b** had a rat FLIPR IC₅₀ value of 160 nM. On the basis of these promising results, we introduced more elaborate substituents at that benzylic position (Table 1). A study of aminoalkyl (**5c**, **5h**, and **5k**) and Boc-aminoalkyl (**5d**, **5f**, **5i**, and **5l**) groups indicated that rat UT antagonist potency was optimal with one to three methylenes in the linker and suggested that human UT potency was optimal with three methylenes in the linker. A follow-up study of 2-thienylsulfonamidoalkyl

Table 1. Urotensin-II Receptor Functional and Binding Data for Phthalimides^a


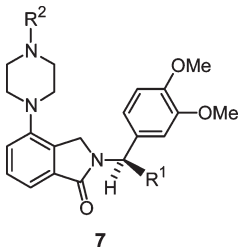
compd	R ¹	R ²	rat FLIPR ^b IC ₅₀ , nM	hUT bdg ^c K _i , nM	human FLIPR ^d IC ₅₀ , nM
2	H	2,6-F ₂ C ₆ H ₃ CH ₂	1000	310	
3	H	PhCH ₂	150	160	
(<i>R</i>)- 4	H	(<i>R</i>)-Ph(Me)CH	84	570	1900
(<i>S</i>)- 4	H	(<i>S</i>)-Ph(Me)CH	490		
5a	Me	(<i>R</i>)-Ph(Me)CH	70	310	
(<i>R,R</i>)- 5a	(<i>R</i>)-Me	(<i>R</i>)-Ph(Me)CH	150	230	
(<i>R,S</i>)- 5a	(<i>S</i>)-Me	(<i>R</i>)-Ph(Me)CH	130	160	
5b	Et	(<i>R</i>)-Ph(Me)CH	180	310	
5c	CH ₂ NH ₂	(<i>R</i>)-Ph(Me)CH	300	700	
5d	CH ₂ NH-Boc	(<i>R</i>)-Ph(Me)CH	120	430	
5e	CH ₂ NH-SO ₂ -Th	(<i>R</i>)-Ph(Me)CH	75	290	
5f	(CH ₂) ₂ NH-Boc	(<i>R</i>)-Ph(Me)CH	110	540	
5g	(CH ₂) ₂ NH-SO ₂ -Th	(<i>R</i>)-Ph(Me)CH	120	270	
5h	(CH ₂) ₃ NH ₂	(<i>R</i>)-Ph(Me)CH	200	3200	
5i	(CH ₂) ₃ NH-Boc	(<i>R</i>)-Ph(Me)CH	200	200	
5j	(CH ₂) ₃ NH-SO ₂ -Th	(<i>R</i>)-Ph(Me)CH	80	76	250
(<i>R,S</i>)- 5j	(CH ₂) ₃ NH-SO ₂ -Th	(<i>R</i>)-Ph(Me)CH	69	120	260
(<i>R,R</i>)- 5j ^e	(CH ₂) ₃ NH-SO ₂ -Th	(<i>R</i>)-Ph(Me)CH	29	49	240
5l	(CH ₂) ₄ NH-Boc	(<i>R</i>)-Ph(Me)CH	65000	> 10000	
5m	(CH ₂) ₃ NH-SO ₂ Me	(<i>R</i>)-Ph(Me)CH	110	1400	
5n	(CH ₂) ₃ NH-SO ₂ -ClTh	(<i>R</i>)-Ph(Me)CH	1700		
6a	(CH ₂) ₃ NH-SO ₂ -Th	H	40	150	500
6b	(CH ₂) ₃ NH-SO ₂ -Th	Me	16	59	220
6c	(CH ₂) ₃ NH-SO ₂ -Th	Et	4.8	35	150
6d	(CH ₂) ₃ NH-SO ₂ -Th	<i>i</i> -Pr	3.5	45	150
6e	(CH ₂) ₃ NH-SO ₂ -Isox	(<i>R</i>)-Ph(Me)CH	20	32	130
6f	(CH ₂) ₃ NH-C(O)-Isox	(<i>R</i>)-Ph(Me)CH	11	130	760
6g	(CH ₂) ₃ NH-SO ₂ -Pylz	(<i>R</i>)-Ph(Me)CH	11	13	47
6h	(CH ₂) ₃ NH-C(O)-Pylz	(<i>R</i>)-Ph(Me)CH	11	87	37
6i	(CH ₂) ₃ NH-SO ₂ -Imid	(<i>R</i>)-Ph(Me)CH	14	16	220
6j	(CH ₂) ₃ NH-SO ₂ -Imid	Et	140	97	810
8 ^f			34	8.0	8.0
9 ^g			> 75000	41	320

^a Target compounds were purified either by silica gel flash-column chromatography (230–400 mesh) or HPLC on a Gilson instrument equipped with a reverse-phase Kromasil C18 column (10 μ , 250 mm \times 50 mm). All compounds were characterized by ESI-MS and 300 MHz ¹H NMR. Abbreviations: Th, 2-thienyl; ClTh, 5-chlorothien-2-yl; Isox, 5-methylisoxazol-4-yl; Imid, 1,2-dimethylimidazol-4-yl; Pylz, 3,5-dimethylpyrazol-4-yl.

^b Inhibition of calcium mobilization in CHO-K1 cells transfected with the rat UT, as measured by FLIPR ($N = 2-6$). ^c Inhibition of [¹²⁵I]U-II binding to UT in cultured human rhabdomyosarcoma cells (RMS13) ($N = 2$). ^d Inhibition of calcium mobilization in human rhabdomyosarcoma cells, as measured by FLIPR ($N = 2-6$). ^e Corresponds to structure type **6**. ^f Reference standard SB-706375 (ref 26; also Dhanak, D.; Gallagher, T. F.; Knight, S. D. PCT Int. Appl. WO 2002089792, 2002). ^g Reference standard palosuran (ref 17i; also Aissaoui, H., et al. PCT Int. Appl. WO 2003048154, 2003).

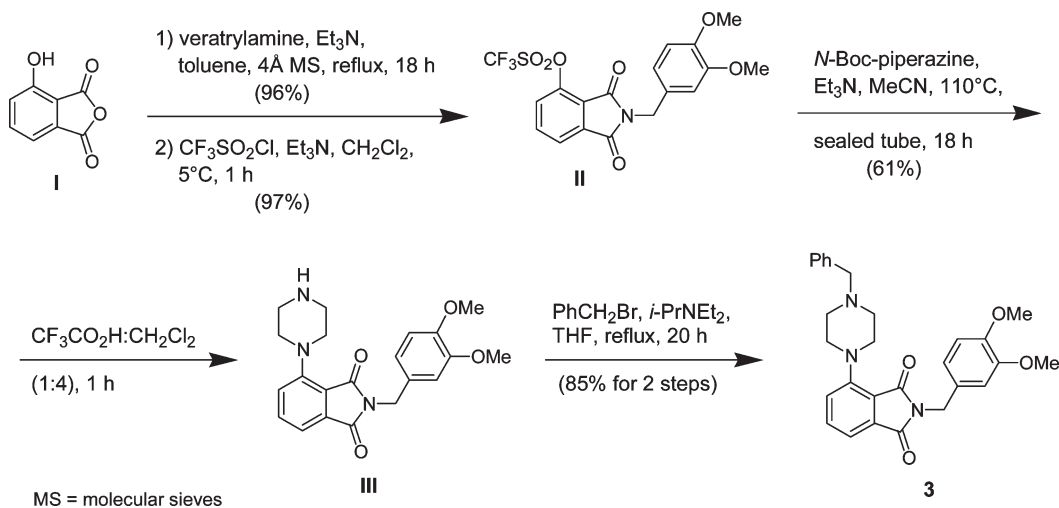
groups with one to three methylenes (**5e**, **5g**, and **5j**) confirmed that a three-carbon linker leads to better human UT antagonist potency (hUT $K_i = 290$, 270, and 76 nM, respectively). Methylsulfonamide **5m** and, especially, (5-chlorothienyl)sulfonamide **5n** showed attenuated potency. Given that such derivatization could yield good antagonist potency against both rat and human receptors, numerous sulfonamides with a three-carbon linker were examined in our rat and human FLIPR-based functional assays and for human UT binding (see Experimental Section). Two notable subunits were (5-Me-oxazol-4-yl)SO₂NH(CH₂)₃– (rat FLIPR IC₅₀/hUT K_i /human FLIPR IC₅₀ = 14/31/46 nM) and MeSO₂CH₂SO₂NH(CH₂)₃– (19/25/250 nM), which improved upon **5j** (80/76/250 nM).

At this juncture, we pursued the evaluation of single diastereomers only. Although the enantiomers (*R,S*)-**5j** and (*R,R*)-**5j** did not have distinctly different potencies, there was a potency bias for the (*R,R*)-isomer over the (*R,S*)-isomer (Table 1). Thus, diverse derivatives with the (*R,R*) structure were synthesized and tested, and a sampling of our large number of analogues is presented in Table 1. It was found that ethyl (**6c**) and isopropyl (**6d**) are optimal groups for the piperazine nitrogen, thereby attaining single-digit nanomolar rat UT antagonist potency. A carboxamide functionality could replace the sulfonamide, albeit with an attenuation in potency (cf. **6e** and **6f**; **6g** and **6h**). The piperazine N-substituent and the sulfonamide group did not necessarily combine in an additive manner (cf. **6i** and **6j**).

Table 2. Urotensin-II Receptor Functional and Binding Data for Isoindolinones^a


compd	R ¹	R ²	rat FLIPR ^b IC ₅₀ , nM	hUT bdg ^c K _i , nM	human FLIPR ^d IC ₅₀ , nM
7a	(CH ₂) ₃ NH-SO ₂ -Th	Et	1.0	4.0	8.0
7b	(CH ₂) ₃ NH-SO ₂ -Th	<i>i</i> -Pr	3.0	4.0	53
7c	(CH ₂) ₃ NH-C(O)-Th	Et	7.0	18	140
7d	(CH ₂) ₃ NH-CH ₂ -Th	Et	6.0	18	59
7e	(CH ₂) ₃ NMe-SO ₂ -Th	Et	7.0	< 5	88
7f	(CH ₂) ₃ NMe-SO ₂ -Th	H	39	49	410
7g	(CH ₂) ₃ NMe-SO ₂ -Th	Me	16	< 6	340
7h	(CH ₂) ₃ NMe-SO ₂ -Th	<i>i</i> -Pr	2.0	11	500
7i	(CH ₂) ₃ NMe-SO ₂ -Th	cyclopropyl	13	59	1200
7j	(CH ₂) ₃ NMe-SO ₂ -Th	cyclobutyl	4.0	44	510
7k	(CH ₂) ₃ NH-C(O)-Pylz	Et	16	11	130
7l	(CH ₂) ₃ NH-C(O)-Isox	(<i>R</i>)-Ph(Me)CH	6.0	15	320
7m	(CH ₂) ₃ NH-SO ₂ -Imid	Et	23	25	51
7n	(CH ₂) ₃ NH-ClPyrm	Et	1.0	62	500
7o	(CH ₂) ₃ NH-MeOPyrm	Et	4.0	8.0	62
8^e			34	8.0	8.0
9^f			> 75000	41	320

^a Target compounds were purified either by silica gel flash-column chromatography (230–400 mesh) or HPLC on a Gilson instrument equipped with a reverse-phase Kromasil C18 column (10 μ , 250 mm \times 50 mm). All compounds were characterized by ESI-MS and 300 MHz ¹H NMR. Abbreviations: Th, 2-thienyl; ClTh, 5-chlorothien-2-yl; Isox, 5-methylisoxazol-4-yl; Imid, 1,2-dimethylimidazol-4-yl; Pylz, 3,5-dimethylpyrazol-4-yl. Additional abbreviations: ClPyrm, 6-chloropyrimidin-2-yl; MeOPyrm, 6-methoxypyrimidin-2-yl. ^b Inhibition of calcium mobilization in CHO-K1 cells transfected with the rat UT, as measured by FLIPR (*N* = 2–6). ^c Inhibition of [¹²⁵I]U-II binding to UT in cultured human rhabdomyosarcoma cells (RMS13) (*N* = 2). ^d Inhibition of calcium mobilization in human rhabdomyosarcoma cells, as measured by FLIPR (*N* = 2–6). ^e Reference standard SB-706375 (ref 26; also Dhanak, D.; Gallagher, T. F.; Knight, S. D. PCT Int. Appl. WO 2002089792, 2002). ^f Reference standard palosuran (ref 17i; also Aissaoui, H., et al. PCT Int. Appl. WO 2003048154, 2003).

Scheme 1. Synthesis of **3**

We extended our investigation to the corresponding isoindolinone analogues, **7** (Table 2), which were assembled from diamine (*R*)-**XVI** according to the route in Scheme 5. The SAR information gained from the phthalimide series was used as a starting point for the isoindolinone series. Thus, we readily obtained some very potent antagonists, several with single-digit nanomolar potencies in the rat FLIPR assay (viz. **7a–e**, **7h**, **7j**, **7l**, **7n**, and **7o**) and some

with single-digit nanomolar affinities in the hUT binding assay (viz. **7a**, **7b**, **7e**, **7g**, and **7o**). Remarkably, **7a** also exhibited very potent functional antagonism in the human calcium flux assay (IC₅₀ = 8.0 nM) (see Experimental Section). The next tier of compounds in this human cellular functional assay were **7b**, **7d**, and **7m** with IC₅₀ values of 50–60 nM. Across our three assays, ethyl was the optimal *N*-alkyl group (R²) for antagonist potency. It is noteworthy

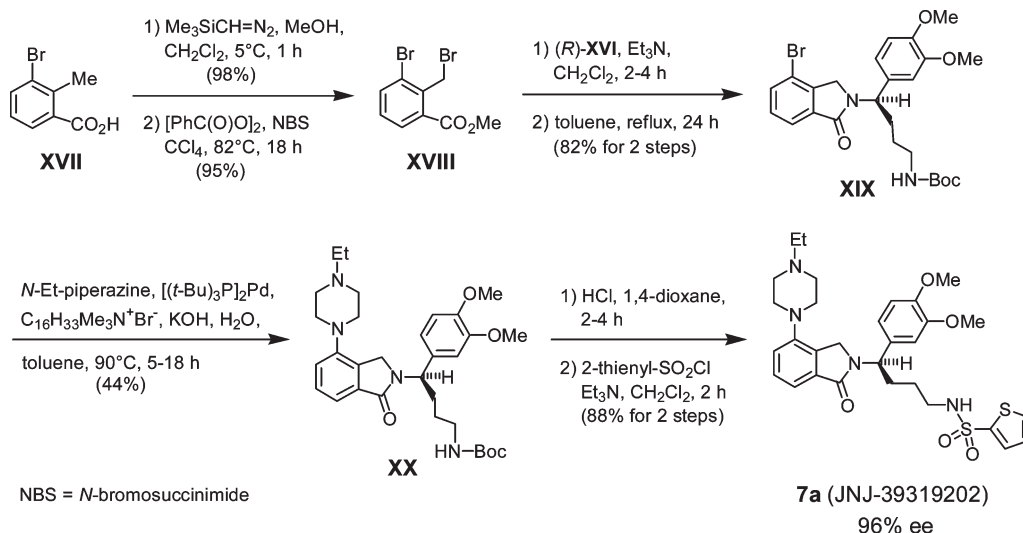
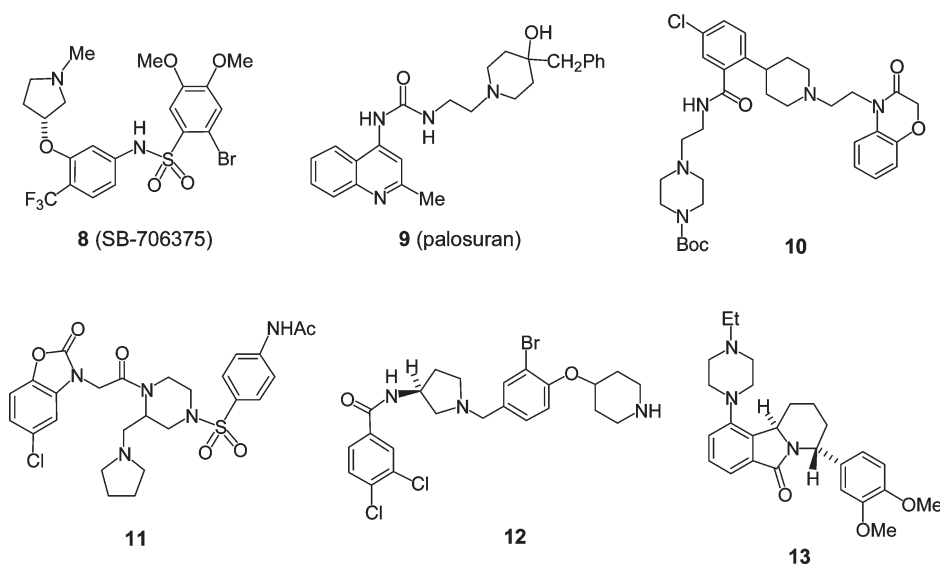
Scheme 5. Synthesis of **7a**

Chart 2. U-II Receptor Antagonist Molecules



antagonist molecules. Compound **7a**, administered iv 15 min prior to administration of U-II, attenuated the increase in ear pinna temperature (whereas vehicle had no effect). Complete reversal with **7a** in this assay was attained at 10 mg/kg (Figure 1), and a similar response was observed with intravenously administered **8**. An area for improvement for **7a** and its congeners would be oral bioavailability, as *F* generally ranged between 10 and 15% in oral PK studies in rats.

To obtain preliminary insight into selectivity for UT over other molecular targets, **7a** was profiled for binding affinity in 50 receptors and ion channels at a high concentration of 10 μ M by CEREP.²⁹ Less than 50% inhibition of the binding of a reference ligand was observed in 90% of the individual assays.³⁰ The following assays showed inhibition values of > 50%: α 1 adrenergic receptor (68%), human M1 muscarinic receptor (65%), human M3 muscarinic receptor (55%), human 5-HT1A serotonin receptor (93%), 5-HT1B serotonin receptor (66%), and Na⁺ channel site 2 (59%).

Different Classes of Nonpeptide U-II Receptor Antagonists. Various U-II receptor antagonist series have been reported.^{15–17}

Our earlier series revolved around phenylpiperidine-benzoxazinones, such as **10**, which also bears a piperazine group with one basic nitrogen center (Chart 2).¹⁵ The series from Actelion was anchored by palosuran (**9**), in which a 4-quinoline is linked to a 4-substituted piperidine,¹⁷ⁱ and GlaxoSmithKline compound **8** contains a 3,4-dimethoxybenzenesulfonamide linked to a pyrrolidine.²⁶ Some other classes of potent U-II antagonists are represented by structures **11**^{17g} and **12**^{17f} (Chart 2). There appears to be some analogy between the subunits of chemotypes **10** and **11**, but their key basic amine centers do not correlate, as discussed further below.

A cursory inspection of structures **7a** and **8–12** suggests that there is no clear-cut structural pattern to describe a common pharmacophore for potent UT antagonist ligands. However, to gain a better appreciation of the pharmacophores for these six series, we generated energy-minimized structures for each representative compound (see Supporting Information) with Maestro³¹ by employing the OPLS-AA force-field³² and a GB/SA water model.³³ Each structure was also subjected to a limited amount of conformational analysis by using the mixed-torsion low-mode algorithm³⁴ in

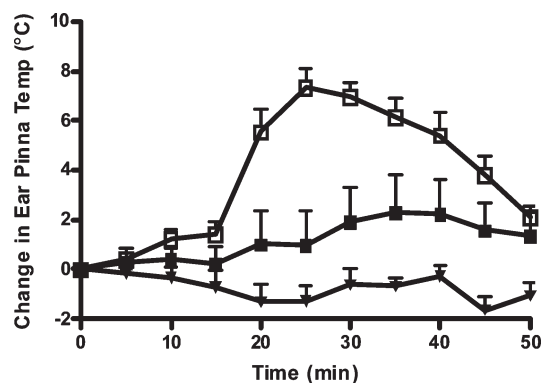


Figure 1. Effects of **7a** on ear pinna temperature over time. A solution of the test compound in 20% aqueous hydroxypropyl- β -cyclodextrin (HPBDC) was administered intravenously at 3 mg/kg (filled squares) or 10 mg/kg (filled, inverted triangles). The administration of vehicle is depicted by open squares. Data are mean temperature changes from baseline \pm SEM ($N = 5$ per group).

Maestro. To assess the relative distances between key interaction sites, a common pharmacophore was generated by using Phase.³⁵ It was only possible to obtain very simple three-point pharmacophores because of the great diversity between these six structures. The distances in the following discussion were derived from low energy conformations aligned according to this rudimentary pharmacophore. All of the chemotypes possess at least one basic amine nitrogen, which was used as a reference frame, and at least two benzenoid subunits, which were used as secondary reference elements. Compound **7a** contains a basic nitrogen center in the piperazine ring that is 5.5 Å from the isoindolinone benzene ring (center of ring), 8.3 Å from the amide carbonyl, 9.9 Å from the key dimethoxybenzene ring (center of ring), and 6.7 Å from the sulfonamide NH, with the dimethoxybenzene ring (center of ring) \sim 6.5 Å from the other benzene ring, 3.6 Å from the amide carbonyl, and 6.4 Å from the sulfonamide NH. Considering **8–12**, they all contain a basic amine nitrogen, as a pyrrolidine, piperidine, piperidine/piperazine, pyrrolidine, and piperidine/pyrrolidine, respectively, and they all contain at least one aromatic ring that is proximal to the amine center and nearby amide groups. Our series needed the 3,4-dimethoxybenzene subunit for strong antagonist potency, and this subunit is also present in **8**; however, it is absent from the series represented by **9–12**. The basic center in **8** is 5.6 Å from the dimethoxybenzene ring (center of ring), 8.4 Å from the sulfonamide NH, and 6.0 Å from another aromatic ring. The basic center in **9** is 6.4 Å from an aromatic ring (center of ring), 8.9 Å from the bicyclic aromatic group in the opposite direction, and 4.5 Å from the urea carbonyl. There are two basic amine centers in **10**, separated by \sim 10 Å. The benzoxazinone benzene ring is 5.4 Å from the piperidine nitrogen and \sim 15 Å from the basic piperazine nitrogen; the benzamide benzene ring is 5.2 Å from the piperidine nitrogen and 7.3 Å from the piperazine amine nitrogen; the piperidine nitrogen is 4.5 Å from the benzoxazine carbonyl and 5.7 Å from the amide carbonyl; the piperazine amine is 5.0 Å from the Boc carbonyl and 4.5 Å from the amide carbonyl. The basic center in **11** is 7.8 Å from the benzoxazolidinone benzene ring and \sim 6 Å from the benzenesulfonyl ring; each amide carbonyl is 5.7, 5.8, and 6.7 Å from the amine center. The pyrrolidine nitrogen in **12** is 7.3 Å from the benzamide ring and 3.8 Å from the benzyl ring; the piperidine nitrogen is 6.6 Å from the benzyl ring and

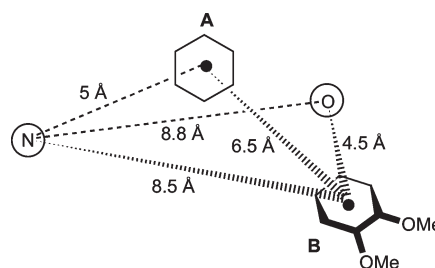


Figure 2. Spatial arrangement and distances for loci in the ground-state conformation of tricycle **13**. The basic piperazine nitrogen (N), carbonyl oxygen (O), and center of the isoindolinone benzene ring (A) are coplanar, while the center of the dimethoxybenzene (B) projects forward from that defined plane.

\sim 17 Å from the benzamide ring; the amide carbonyl is 4.6 Å from the pyrrolidine nitrogen and \sim 14.5 Å from the piperidine nitrogen. This comparative analysis, albeit less than rigorous, suggests that several pharmacophore models can satisfy the requirements for U-II receptor binding and antagonism. A caveat to this analysis would be that we have only considered unbound, ground-state conformations (global energy minima), whereas receptor-bound conformations may be different and more relevant. Given this assessment, it would appear that effective UT antagonists are likely to emanate from diverse chemical entities with specific pharmacophore components related to those that are highlighted.

A key issue in dealing with ligands **7a** and **8–12** to establish understanding about UT pharmacophore models is the conformational freedom available to these molecules. Their wide structural variation also poses a problem. It would be useful to consider a UT ligand with much less conformational dimensionality. Fortunately, we identified tricyclic compound **13** as a potent UT antagonist (rat FLIPR $IC_{50} = 14$ nM; human UT binding $K_i = 64$ nM), which is quite conformationally constrained (Chart 2).³⁶ In its ground-state conformation, **13** has its basic amine nitrogen 5.5 Å from the isoindolinone benzene ring (center of ring), \sim 9 Å from the amide carbonyl, and \sim 10 Å from the dimethoxybenzene ring (center of ring), with the dimethoxybenzene ring spaced 4.5 Å from the amide carbonyl and the two benzene rings (centers) separated by 6.5 Å (Figure 2). Many of these dimensions correspond to the dimensions in **7a** (disregarding the sulfonamide group).

On the basis of antagonist structures known through 2005, Carotenuto et al. described two general pharmacophores in terms of a basic amine linked to an aryl-1 and to an aryl-2 group, or an aryl-1 linked to an aryl-2 that is then linked to a basic amine.^{16b} Lescot et al. also developed more than one antagonist pharmacophore, which suggests a lack of convergence between the antagonist ligands that were considered.³⁷ They advanced two different models comprised of two aromatic rings, one hydrophobic group, a basic amine center, and a hydrogen-bond acceptor, each with a different spatial arrangement.³⁷ Consequently, there would seem to be general agreement that UT antagonist structures can be achieved through more than one pharmacophore model. Given that **13** has a fairly well-defined spatial geometry, because of its conformational constraints,³⁶ it serves to define one type of UT antagonist pharmacophore.

Conclusion

We have discovered two related series of nonpeptide U-II receptor antagonists based on piperazino-phthalimide

(5 and 6) and piperazino-isoindolinone (7) scaffolds. Compound 7a was found to be an exceedingly potent U-II receptor antagonist in vitro, and it also blocked the effects of U-II in vivo in the rat ear-flush model. Structure types 6 and 7 are very distinctive relative to the structure types for other nonpeptide U-II receptor antagonist series, such as those represented by 8²⁶ and palosuran (9).¹⁷ⁱ Our series required the 3,4-dimethoxybenzene subunit for robust antagonist potency, and this structural element is also present in 8. However, the series represented by 9–12 do not possess this subunit. In any case, potent UT antagonists contain at least one basic amine nitrogen and at least two benzenoid subunits, with one aromatic ring being proximal to the amine center, as well as amide groups near the amine center. Interestingly, such structural elements are contained within the U-II agonist pharmacophore, although with much different distances.³ At this juncture, we can conclude that several pharmacophore models will satisfy the requirements for U-II receptor binding and antagonist action.

Experimental Section

General Chemical Procedures. ¹H NMR spectra were generally acquired at 300.14 MHz on a Bruker Avance-300 spectrometer in CDCl₃ with Me₄Si as an internal standard, unless indicated otherwise. The 400-MHz ¹H NMR spectra were recorded with a Bruker AC-400 spectrometer with Me₄Si as an internal standard. Electrospray (ES) mass spectra were obtained on a Micromass Platform LC single quadrupole mass spectrometer in the positive mode. The structures of all new compounds were consistent with their ¹H NMR and ES-MS mass spectra. Analytical HPLC analyses were performed on an Agilent series 1100 HPLC instrument eluting with a gradient of water/MeCN/TFA (10:90:0.2 to 90:10:0.2) over 4 min with a flow rate of 0.75 mL/min on a Kromasil C18 column (50 mm × 2.0 mm; 3.5 μm particle size) or on a Supelcosil ABZ+Plus column (50 mm × 2.0 mm; 3.5 μm particle size) at 32 °C, with signals being recorded simultaneously at 220 and 254 nm with a diode-array detector. These HPLC analyses served as the principal determinant of compound purity, which was >95% for target compounds. The measured purity for target compounds is given in parentheses throughout the Experimental Section. Normal-phase preparative chromatography was performed on an Isco Combiflash Separation System Sg 100c equipped with a Biotage FLASH Si 40 M silica gel cartridge (KP-Sil Silica, 32–63 μ, 60 Å; 4 cm × 15 cm) eluting at 35 mL/min with detection at 254 nm. Reversed-phase preparative chromatography was performed on a Gilson HPLC with a reversed-phase Kromasil column (10 μ, 100 Å C18, column length 250 mm × 50 mm). Optical rotations were measured on a Perkin-Elmer 241 polarimeter. Elemental analysis and Karl Fischer water analysis were determined for certain specific compounds by Quantitative Technologies Inc., Whitehouse, NJ.

Synthesis of 4-Hydroxy-2-(3,4-dimethoxybenzyl)-1,3-dioxo-2,3-dihydro-1H-isoindol-4-yl Trifluoromethanesulfonic Acid Ester (II). A 200 mL round-bottom flask was charged with 4-hydroxy-2,3-dihydro-1H-isobenzofuran-1,3-dione (3.07 g, 0.019 mol) and dry toluene (94 mL). Veratrylamine (2.8 mL, 0.019 mol) and triethylamine (3.6 mL, 0.026 mol) were added to the mixture. A Dean-Stark trap filled with 4A molecular sieves was attached to the flask and the mixture was refluxed for 24 h. The mixture was cooled to room temperature and diluted with CH₂Cl₂ (200 mL) and washed with 1 N HCl (100 mL). The organic layers were combined and dried using MgSO₄, filtered through celite, and concentrated in vacuo to give 5.6 g (96%) of a yellow solid. ¹H NMR δ 7.70–7.86 (m, 1 H), 7.57 (overlapping dd, *J* = 7.5 Hz, 1 H), 7.37 (d, *J* = 7.3 Hz, 1 H), 7.15 (d, *J* = 8.4 Hz, 1 H), 6.91–7.01 (m, 2 H), 6.81 (d, *J* = 7.8 Hz, 1 H), 4.74 (s, 2 H), 3.88 (s, 3 H), 3.85 (s, 3 H). MS (ES⁺) 314 (M + 1). HPLC: Kromasil C18 column (50 mm × 2 mm; 3.5 μ,

gradient 10–90% (MeCN + 0.16% TFA) in (water + 0.2% TFA) over 4 min, *t*_R = 3.38 min (98%). A 500 mL round-bottom flask containing 4-hydroxy-2-(3,4-dimethoxybenzyl)-2,3-dihydro-1H-isoindole-1,3-dione (5.90 g, 0.019 mol), CH₂Cl₂ (80 mL), and Et₃N (3.6 mL, 0.026 mol) was cooled using an ice–water bath. A solution of trifluoromethanesulfonyl chloride (2.2 mL, 0.021 mol) in CH₂Cl₂ (20 mL) was added dropwise via an addition funnel. The mixture was then stirred for 1 h in an ice–water bath. The mixture was then diluted with CH₂Cl₂ (200 mL) and washed with 1 N HCl (100 mL). The organic layer was dried using MgSO₄, filtered through celite, and concentrated in vacuo to give 8.20 g (97%) of II as a yellow solid. ¹H NMR δ 7.78–7.87 (m, 2 H), 7.53 (d, *J* = 8.3 Hz, 1 H), 6.99–7.02 (m, 2 H), 6.79 (d, *J* = 8.1 Hz, 1 H), 4.79 (s, 2 H), 3.87 (s, 3 H), 3.84 (s, 3 H). MS (ES⁺) 446 (M + 1). HPLC: Kromasil C18 column (50 mm × 2 mm; 3.5 μ), gradient 10–90% (MeCN + 0.16% TFA) in (water + 0.2% TFA) over 4 min, *t*_R = 4.14 min (96%).

General Synthesis of Compounds 2 and 3. 4-[4-(Benzyl)piperazin-1-yl]-2-(3,4-dimethoxybenzyl)-2,3-dihydro-1H-isoindole-1,3-dione (3). A 10 mL sealed-tube reactor was charged with II (0.50 g, 1.12 mmol), 1-Boc-piperazine (0.22 g, 1.18 mmol), toluene (1.3 mL), and Et₃N (0.2 mL, 1.43 mmol). The tube was sealed under argon and heated to 110 °C for 18 h. The mixture was cooled to 23 °C and purified via flash silica gel chromatography (230–400 mesh silica gel 60, 80:20 hexanes:ethyl acetate) to give 0.33 g (61%) of a yellow solid. ¹H NMR (300 MHz, MeOH) δ 7.67 (overlapping dd, *J* = 7.2 Hz, 1 H), 7.38 (d, *J* = 7.2 Hz, 1 H), 7.28 (d, *J* = 8.2 Hz, 1 H), 6.99 (s, 1 H), 6.86–6.93 (m, 2 H), 4.71 (s, 2 H), 3.81 (s, 3 H), 3.79 (s, 3 H), 3.61–3.65 (m, 4 H), 3.27–3.31 (m, 4 H), 1.48 (s, 9 H). MS (ES⁺) 482 (M + 1). A 50 mL round-bottom flask containing 4-[2-(3,4-dimethoxybenzyl)-1,3-dioxo-2,3-dihydro-1H-isoindol-4-yl]-piperazine-1-carboxylic acid *tert*-butyl ester (0.33 g, 0.69 mmol) and CH₂Cl₂ (3.0 mL) was treated with TFA (0.7 mL) and the mixture was stirred at 23 °C for 1 h. The mixture was concentrated in vacuo, and the crude oil was dissolved in THF (3.4 mL). Benzyl bromide (0.12 mL, 0.97 mmol) and diethylisopropylamine (0.26 mL, 1.49 mmol) were added. The mixture was heated at reflux for 24 h and evaporated. The crude oil was purified on a Gilson HPLC with a reversed phase Kromasil C18 column (gradient 80:20–0:100 H₂O:MeCN) to give 369 mg (85%) of 3 as a yellow solid. ¹H NMR δ 7.60 (overlapping dd, *J* = 7.4 Hz, 1 H), 7.39–7.50 (m, 6 H), 7.12 (d, *J* = 8.2 Hz, 1 H), 6.90–6.97 (m, 2 H), 6.37 (d, *J* = 8.7 Hz, 1 H), 4.72 (s, 2 H), 4.27 (s, 2 H), 3.87 (s, 3 H), 3.83 (s, 3 H), 3.66–3.77 (m, 4 H), 3.41–3.48 (m, 2 H), 3.14–3.18 (m, 2 H). MS (ES⁺) 472 (M + 1). HPLC: Kromasil C18 column (50 mm × 2 mm; 3.5 μ), gradient 10–90% (MeCN + 0.16% TFA) in (water + 0.2% TFA) over 4 min, *t*_R = 3.21 min (99%).

General Synthesis of Compounds 4 and 5b–n. N-(2-Thiophenesulfonyl)-[4-(3,4-dimethoxyphenyl)]-4-{1,3-dioxo-4-[4-(1-phenylethyl)piperazin-1-yl]-2,3-dihydro-1H-isoindol-2-yl]butyl}amide (5j). A 500 mL round-bottom flask containing DMF (207 mL) and 4-*tert*-butoxycarbonylaminobutyric acid (4.2 g, 20.6 mmol) was cooled using an ice–water bath. Triethylamine (8.8 mL, 63.1 mmol) was added, followed by the benzotriazol-1-yloxy-tris(dimethylamino)phosphonium (BOP) hexafluorophosphate (10.0 g, 22.6 mmol) and *N,O*-dimethylhydroxylamine hydrochloride (3.1 g, 31.8 mmol). The mixture was stirred at room temperature for 24 h, diluted with CH₂Cl₂ (500 mL), and transferred to a separatory funnel. The organic layer was washed with 1 N HCl (300 mL) and water (2 × 300 mL). The organic layer was dried using MgSO₄, filtered through celite, concentrated in vacuo, and purified via flash chromatography (230–400 mesh silica gel 60, gradient 100:0–90:10 CH₂Cl₂:MeOH) to give 5.08 g of [3-(methoxymethylcarbamoyl)propyl]carbamic acid *tert*-butyl ester as a white solid (91%). ¹H NMR δ 3.65 (s, 3 H), 3.22–3.21 (m, 2 H), 3.16 (s, 3 H), 2.45–2.54 (m, 2 H), 1.80–1.89 (m, 2 H), 1.42 (s, 9 H). HPLC: Kromasil C18 column (50 mm × 2 mm; 3.5 μ), gradient 10–90% (MeCN + 0.16% TFA) in (water + 0.2% TFA) over 4 min, *t*_R = 2.74 min (97%). A 1 L round-bottom flask

containing this material (5.09 g, 20.7 mmol) and tetrahydrofuran (415 mL) was cooled by using an ice–water bath. A solution of 3,4-dimethoxyphenylmagnesium bromide in THF (207 mL, 104 mmol) was added dropwise via an addition funnel over 30 min. The mixture was allowed to warm to room temperature and stirred for 20 h. Water (150 mL) was added, and the mixture was concentrated in vacuo, extracted with CH₂Cl₂ (600 mL), and washed with water (2 × 300 mL). The organic layer was dried with MgSO₄, filtered through celite, concentrated in vacuo, and purified via flash chromatography (230–400 mesh silica gel 60, gradient 90:10–50:50 hexanes:ethyl acetate) to give 4.0 g of [4-(3,4-dimethoxyphenyl)-4-oxo-butyl]carbamic acid *tert*-butyl ester [V, R¹ = (CH₂)₃NH-Boc], as a white solid (60%). ¹H NMR δ 7.57 (d, *J* = 8.2 Hz, 1 H), 7.52 (s, 1 H), 6.88 (d, *J* = 8.6 Hz, 1 H), 3.95 (s, 3 H), 3.92 (s, 3 H), 3.27–3.34 (m, 2 H), 2.97–3.02 (m, 2 H), 1.92–1.99 (m, 2 H), 1.42 (s, 9 H). HPLC: Kromasil C18 column (50 mm × 2 mm; 3.5 μ), gradient 10–90% (MeCN + 0.16% TFA) in (water + 0.2% TFA) over 4 min, *t*_R = 3.48 min (98%). A 300 mL round-bottom flask was charged with this material (4.0 g, 12.4 mmol), ammonium acetate (9.5 g, 123.2 mmol), and methanol (42.0 mL). Sodium cyanoborohydride (0.55 g, 8.8 mmol) was added, and the mixture was heated at 40 °C for 22 h. The mixture was cooled to room temperature, and 1 N NaOH (200 mL) was added. The mixture was transferred to a separatory funnel and extracted with CH₂Cl₂ (3 × 200 mL). The organic layer was dried with MgSO₄, filtered through celite, concentrated in vacuo, and purified via flash chromatography (230–400 mesh silica gel 60, gradient 100:0–90:10 CH₂Cl₂:MeOH) to give 2.0 g of [4-amino-4-(3,4-dimethoxyphenyl)butyl]carbamic acid *tert*-butyl ester [VI, R¹ = (CH₂)₃NH-Boc], as a white solid (50%). ¹H NMR δ 6.83–6.87 (m, 3 H), 4.53–4.60 (m, 1 H), 3.90 (s, 3 H), 3.87 (s, 3 H), 3.10–3.15 (m, 2 H), 1.63–1.71 (m, 5 H), 1.43 (s, 9 H). HPLC: Kromasil C18 column (50 mm × 2 mm; 3.5 μ), gradient 10–90% (MeCN + 0.16% TFA) in (water + 0.2% TFA) over 4 min, *t*_R = 2.84 min (97%). To a 50 mL round-bottom flask containing 4-hydroxy-2,3-dihydro-1*H*-isobenzofuran-1,3-dione (1.1 g, 6.70 mmol) and dry toluene (30 mL) was added [4-amino-4-(3,4-dimethoxyphenyl)butyl]carbamic acid *tert*-butyl ester (2.2 g, 6.79 mmol) and triethylamine (1.2 mL, 8.61 mmol). A Dean–Stark trap filled with 4A molecular sieves was attached to the flask and the mixture was refluxed for 24 h. The mixture was cooled to room temperature, diluted with CH₂Cl₂ (200 mL), and washed with 1 N HCl (100 mL). The organic layer was dried (MgSO₄), filtered through celite, and concentrated in vacuo to give 3.1 g (98%) of [4-(3,4-dimethoxyphenyl)-4-(4-hydroxy-1,3-dioxo-2,3-dihydro-1*H*-isoindol-2-yl)butyl]carbamic acid *tert*-butyl ester [VII, R¹ = (CH₂)₃NH-Boc], as a yellow solid. ¹H NMR δ 7.66–7.70 (m, 1 H), 7.52–7.57 (m, 1 H), 7.06–7.16 (m, 1 H), 6.79–6.88 (m, 3 H), 5.16–5.21 (m, 1 H), 3.88 (s, 3 H), 3.85 (s, 3 H), 3.06–3.19 (m, 1 H), 2.49–2.56 (m, 1 H), 2.26–2.33 (m, 1 H), 1.46–1.56 (m, 2 H), 1.42 (s, 9 H). HPLC: Kromasil C18 column (50 mm × 2 mm; 3.5 μ), gradient 10–90% (MeCN + 0.16% TFA) in (water + 0.2% TFA) over 4 min, *t*_R = 3.94 min (97%). A 500 mL round-bottom flask containing this material (6.60 g, 0.014 mol), CH₂Cl₂ (60 mL), and Et₃N (2.3 mL, 0.017 mol) was cooled using an ice–water bath. A solution of trifluoromethanesulfonyl chloride (1.6 mL, 0.015 mol) in CH₂Cl₂ (10 mL) was added dropwise via an addition funnel. The mixture was stirred for 1 h in an ice–water bath. The mixture was diluted with CH₂Cl₂ (200 mL), washed with 1 N HCl (100 mL), and saturated aqueous sodium bicarbonate (1 × 100 mL). The organic layer was dried using MgSO₄, filtered through celite, and concentrated in vacuo to give 7.06 g (84%) of triflate as a yellow solid. ¹H NMR δ 7.76–7.83 (m, 2 H), 7.51 (d, *J* = 7.8 Hz, 1 H), 7.07–7.12 (m, 2 H), 6.80 (d, *J* = 8.0 Hz, 1 H), 5.22–5.27 (m, 1 H), 3.88 (s, 3 H), 3.85 (s, 3 H), 3.16–3.26 (m, 2 H), 2.42–2.59 (m, 1 H), 2.29–2.40 (m, 1 H), 1.55–1.66 (m, 2 H), 1.42 (s, 9 H). MS (ES⁺) 603 (M + 1). HPLC: Kromasil C18 column (50 mm × 2 mm; 3.5 μ), gradient 10–90% (MeCN + 0.16% TFA) in (water + 0.2% TFA) over 4 min, *t*_R = 4.72 min (96%). A 50 mL sealed-tube vessel was charged with this material (7.53 g, 0.013 mol), 1-[(*R*)-1-phenylethyl]piperazine (2.50 g, 0.013 mol), toluene (13 mL), and Et₃N (2.4

mL, 0.017 mol). The tube was sealed under argon and heated to 110 °C for 21 h. The mixture was cooled to room temperature and purified via flash silica gel chromatography (230–400 mesh silica gel 60, 80:20 hexanes:ethyl acetate) to give 4.61 g (57%) of (4-(3,4-dimethoxyphenyl)-4-{1,3-dioxo-4-[4-(1-phenylethyl)piperazin-1-yl]-2,3-dihydro-1*H*-isoindol-2-yl}butyl)carbamic acid *tert*-butyl ester (**5i**) as a yellow solid. ¹H NMR δ 7.48–7.54 (m, 1 H), 7.23–7.36 (m, 7 H), 7.07–7.11 (m, 2 H), 6.78 (d, *J* = 8.2 Hz, 1 H), 5.18–5.23 (m, 1 H), 4.08–4.16 (m, 1 H), 3.87 (s, 3 H), 3.83 (s, 3 H), 3.26–3.45 (m, 4 H), 3.14–3.22 (m, 2 H), 2.72–2.76 (m, 2 H), 2.55–2.64 (m, 2 H), 2.44–2.52 (m, 1 H), 2.23–2.30 (m, 1 H), 1.38–1.54 (m, 14 H). MS (ES⁺) 643 (M + 1). HPLC: Kromasil C18 column (50 mm × 2 mm; 3.5 μ), gradient 10–90% (MeCN + 0.16% TFA) in (water + 0.2% TFA) over 4 min, *t*_R = 3.31 min (97%). A 50 mL round-bottom flask was charged with **5i** (1.90 g, 2.95 mmol) and 1,4-dioxane (15 mL). A solution of 4 N HCl in 1,4-dioxane (10 mL) was added, and the mixture was stirred at room temperature for 4 h. The mixture was concentrated in vacuo to give **5h**. ¹H NMR (300 MHz, CD₃OD) δ 7.63–7.68 (m, 1 H), 7.51–7.61 (m, 5 H), 7.41 (d, *J* = 7.2 Hz, 1 H), 7.28 (d, *J* = 7.9 Hz, 1 H), 7.13 (s, 1 H), 7.04 (d, *J* = 6.5 Hz, 1 H), 6.89 (d, *J* = 8.4 Hz, 1 H), 5.22–5.27 (m, 1 H), 4.46–4.57 (m, 1 H), 3.82 (s, 3 H), 3.80 (s, 3 H), 3.47–3.66 (m, 4 H), 3.13–3.26 (m, 2 H), 2.96–3.07 (m, 2 H), 2.57–2.67 (m, 1 H), 2.32–2.42 (m, 1 H), 1.80 (d, *J* = 6.8 Hz, 1 H), 1.64–1.74 (m, 2 H), 1.29–1.35 (m, 2 H). MS (ES⁺) 543 (M + 1). HPLC: Kromasil C18 column (50 mm × 2 mm; 3.5 μ), gradient 10–90% (MeCN + 0.16% TFA) in (water + 0.2% TFA) over 4 min, *t*_R = 2.44 min (98%). The solid (1.0 g, 1.63 mmol) was dissolved in CH₂Cl₂ (8.2 mL). Triethylamine (0.7 mL, 5.02 mmol) was added followed by 2-thiophenesulfonyl chloride (0.37 g, 2.03 mmol). The mixture was stirred at room temperature for 24 h and concentrated in vacuo. The crude oil was purified on a Gilson HPLC with a reverse-phase Kromasil C18 column (gradient 80:20–0:100 H₂O:MeCN). The purified material was dissolved in CH₂Cl₂ (50 mL), treated with 1 N HCl in diethyl ether (10 mL), and concentrated in vacuo. This procedure was repeated two more times to give 1.18 g (96%) of **5j** as a yellow solid. ¹H NMR δ 7.71–7.74 (m, 1 H), 7.51–7.61 (m, 3 H), 7.29–7.38 (m, 6 H), 7.02–7.18 (m, 3 H), 6.73–6.80 (m, 1 H), 5.10–5.17 (m, 1 H), 4.50–4.57 (m, 1 H), 3.86 (s, 3 H), 3.83 (s, 3 H), 3.31–3.39 (m, 4 H), 3.06–3.11 (m, 4 H), 2.65–2.74 (m, 2 H), 2.45–2.55 (m, 1 H), 2.20–2.31 (m, 1 H), 1.58–1.63 (m, 2 H), 1.49 (d, *J* = 6.8 Hz, 3 H). MS (ES⁺) 689 (M + 1). HPLC: Kromasil C18 column (50 mm × 2 mm; 3.5 μ), gradient 10–90% (MeCN + 0.16% TFA) in (water + 0.2% TFA) over 4 min, *t*_R = 2.54 min (100%).

Synthesis of (*R,S*)-5a and (*R,R*)-5a. A 50 mL round-bottom flask was charged with borane-dimethyl sulfide solution in toluene (0.4 mL, 0.8 mmol) and toluene (6.0 mL). Octanol (0.32 mL, 2.01 mmol) was added dropwise to the mixture, and stirring was continued at 34 °C for 1 h. (*S*)-α,α-Diphenyl-2-pyrrolidinemethanol (0.14 g, 0.55 mmol) was dissolved in toluene (6.0 mL) and added to the mixture, followed by stirring for 1 h at 34 °C. Borane-dimethyl sulfide solution in toluene (2.8 mL, 1.40 mmol) was added, followed by dropwise addition of a solution of 3,4-dimethoxyacetophenone (1.0 g, 5.55 mmol) in toluene (6.0 mL) over 1 h via addition funnel. The mixture was cooled to room temperature and quenched with 1 N HCl (20 mL). The mixture was transferred to a separatory funnel and extracted with ethyl acetate (200 mL). The organic layer was washed with sodium bicarbonate (50 mL) and sodium chloride (50 mL). The organic layer was dried using MgSO₄, filtered through celite, and concentrated in vacuo to give 820 mg of (*R*)-1-(3,4-dimethoxyphenyl)ethanol (**X**) as a white solid. ¹H NMR δ 6.82–6.95 (m, 3 H), 4.86 (q, *J* = 3.3 Hz, 2 H), 3.90 (s, 3 H), 3.88 (s, 3 H), 1.83 (s, 1 H), 1.49 (d, *J* = 6.4 Hz, 3 H); [α]_D²⁵ +42.0 (c 1.07, CHCl₃). A 100 mL round-bottom flask containing **X** (0.40 g, 2.20 mmol) and CH₂Cl₂ (11.0 mL) was cooled using an ice–water bath. Triethylamine (0.37 mL, 2.65 mmol) was added to the mixture, followed by the dropwise addition methanesulfonyl chloride (0.19 mL, 2.45 mmol). The mixture was

stirred for 4 h at 0 °C and then washed with 1 N HCl (5 mL). The organic layer was dried with MgSO₄ and filtered through celite. Diallylamine (0.27 mL, 2.19 mmol) and 2,2,6,6-tetramethylpiperidine (0.82 mL, 4.83 mmol) were added to the crude CH₂Cl₂ solution. The mixture was refluxed for 24 h, cooled to room temperature, and concentrated in vacuo. The crude oil was purified via flash chromatography (230–400 mesh silica gel 60, gradient 100:0–98:2 CH₂Cl₂:MeOH) to give 0.4 g of diallyl-[1-(*R*)-(3,4-dimethoxyphenyl)ethyl]amine (**XI**) as a white solid. ¹H NMR δ 6.78–6.87 (m, 3 H), 5.78–5.91 (m, 2 H), 5.09–5.20 (m, 4 H), 4.18 (q, *J* = 6.4 Hz, 2 H), 3.90 (m, 3 H), 3.86 (m, 3 H), 3.00–3.17 (m, 4 H), 1.45 (d, *J* = 6.4 Hz, 3 H). A 50 mL round-bottom flask was charged with **XI** (0.40 g, 1.53 mmol) and CH₂Cl₂ (8.0 mL). Pd₂(dba)₃·CHCl₃ (0.16 g, 0.15 mmol), triphenylphosphine (0.16 g, 6.1 mmol), and 1,3-dimethylbarbituric acid (0.79 g, 5.06 mmol) were added, and the mixture was heated at reflux for 3 h. The mixture was cooled to room temperature, transferred to a separatory funnel, and extracted with 1 N HCl (50 mL). The aqueous layer was basified with 3 N NaOH and extracted with ethyl acetate (200 mL). The organic layer was dried with MgSO₄ and filtered through celite to give 1-(*R*)-(3,4-dimethoxyphenyl)ethylamine (**XII**) as a white solid. ¹H NMR δ 6.74–6.85 (m, 3 H), 3.96–4.08 (m, 1 H), 3.83 (m, 3 H), 3.80 (m, 3 H), 1.87–1.97 (broad s, 2 H), 1.31 (d, *J* = 6.6 Hz, 3 H). Compound (*R,S*)-**5a** was prepared by the general methods for compounds **4** and **5b–n** (vide supra) but employing enantiomerically pure benzylamine **XII** (0.14 g). Compound (*R,S*)-**5a** was isolated as a yellow solid. ¹H NMR δ 7.35–7.54 (m, 7 H), 6.93–7.07 (m, 3 H), 6.73 (d, *J* = 8.6 Hz, 1 H), 5.36 (q, *J* = 7.2 Hz, 1 H), 4.21 (q, *J* = 5.2 Hz, 1 H), 3.79 (s, 3 H), 3.77 (s, 3 H), 3.36–3.64 (m, 6 H), 3.79–3.16 (m, 2 H), 1.83 (d, *J* = 7.0 Hz, 3 H), 1.79 (d, *J* = 7.4 Hz, 3 H). MS (ES⁺) 500 (M + 1); [α]_D²⁵ +13.8 (c 1.18, CH₃OH). HPLC: Kromasil C18 column (50 mm × 2 mm; 3.5 μ), gradient 10–90% (MeCN + 0.16% TFA) in (water + 0.2% TFA) over 4 min, *t*_R = 3.43 min (97%).

Synthesis of [(*R*)-4-Amino-4-(3,4-dimethoxyphenyl)butyl]carbamic Acid *tert*-Butyl Ester (XVI**).** A 1 L round-bottom flask containing [3-(methoxymethylcarbamoyl)propyl]carbamic acid benzyl ester (5.08 g, 20.7 mmol) and tetrahydrofuran (415 mL) was cooled using an ice–water bath. A solution of 3,4-dimethoxyphenylmagnesium bromide in THF (207 mL, 104 mmol) was added dropwise via addition funnel over 30 min. The mixture was allowed to warm to room temperature and stirred for 20 h. Water (150 mL) was added to the mixture and concentrated in vacuo. The mixture was extracted with CH₂Cl₂ (600 mL) and washed with water (2 × 300 mL). The organic layer was dried with MgSO₄, filtered through celite, concentrated in vacuo, and purified via flash chromatography (230–400 mesh silica gel 60, gradient 90:10–50:50 hexanes:ethyl acetate) to give 4.0 g of [4-(3,4-dimethoxyphenyl)-4-oxo-butyl]carbamic acid benzyl ester as a white solid. ¹H NMR δ 7.57 (d, *J* = 8.4 Hz, 1 H), 7.51 (s, 1 H), 7.29–7.44 (m, 5 H), 6.88 (d, *J* = 8.4 Hz, 1 H), 5.08 (s, 2 H), 3.95 (s, 3 H), 3.93 (s, 3 H), 3.27–3.34 (m, 2 H), 2.97–3.02 (m, 2 H), 1.92–2.01 (m, 2 H). MS (ES⁺) 358 (M + 1). HPLC: Kromasil C18 column (50 mm × 2 mm; 3.5 μ), gradient 10–90% (MeCN + 0.16% TFA) in (water + 0.2% TFA) over 4 min, *t*_R = 3.62 min (98%). A 200 mL Schlenk tube was charged with [RuCl₂(benzene)]₂ (2.0 g, 4.0 mmol) and (*R*)-Tol-BINAP (5.7 g, 8.4 mmol). The tube was put under vacuum for 15 min and then backflushed with argon. DMF (133 mL, degassed with argon) was added to the tube, and the mixture was flushed with argon. The tube was sealed off and heated to 100 °C for 10 min (with stirring). The DMF was then removed under high vacuum at 70 °C to give [[(*R*)-Tol-BINAP]RuCl₂(DMF)_x] as a reddish/brown solid.³⁸ A 200 mL sealed tube was charged with [4-(3,4-dimethoxyphenyl)-4-oxo-butyl]carbamic acid benzyl ester (8.66 g, 24.2 mmol), [[(*R*)-Tol-BINAP]RuCl₂(DMF)_x] (2.1 g, 2.5 mmol), ammonium formate (15.3 g, 243 mmol), and a 2.0 M solution of ammonia in methanol (97 mL). The tube was flushed with argon, sealed, and

heated at 85 °C for 22 h. The mixture was cooled to room temperature, and the sealed tube was opened carefully due to the release of pressure from excess ammonia. The mixture was concentrated in vacuo, diluted with 1 N HCl (300 mL) and ethanol (150 mL), heated at reflux for 2 h, cooled to room temperature, and washed with diethyl ether (1 × 500 mL). The aqueous layer was basified with 3 N NaOH to pH > 10. It was extracted by using CH₂Cl₂ (3 × 400 mL), and the organic solution was dried (MgSO₄), filtered through celite, and concentrated in vacuo to give 15.66 g of [4-(*R*)-amino-4-(3,4-dimethoxyphenyl)butyl]carbamic acid benzyl ester **XV** as a white solid. ¹H NMR δ 7.30–7.34 (m, 5 H), 6.81–6.87 (m, 3 H), 5.08 (s, 2 H), 3.83–3.90 (m, 7 H), 3.16–3.22 (m, 2 H), 1.38–1.71 (m, 6 H). MS (ES⁺) 359 (M + 1). Daicel Chiralpak AD-H, 4.6 mm × 15 cm, hexanes:2-propanol:Et₂NH (86:14:0.1), 1.0 mL/min; (*S*)-enantiomer 13.57 min, (*R*)-enantiomer 15.67 min; 96% ee. A 500 mL round-bottom flask containing **XV** (15.66 g, 0.044 mol) and CH₂Cl₂ (220 mL) was cooled using an ice–water bath. Triethylamine (7.4 mL, 0.053 mol) was added, followed by the dropwise addition of trifluoroacetic anhydride (6.8 mL, 0.049 mol). After 3 h, the mixture was extracted with CH₂Cl₂ (200 mL) and washed with 1 N HCl (1 × 100 mL), 1 N NaOH (1 × 100 mL), and water (1 × 100 mL). The organic layer was dried with MgSO₄, filtered through celite, and concentrated in vacuo to give 19.49 g (98%) of [4-(3,4-dimethoxyphenyl)-4-(*R*)-(2,2,2-trifluoroacetyl-amino)butyl]carbamic acid benzyl ester as a white solid. ¹H NMR δ 7.31–7.35 (m, 5 H), 6.80–6.89 (m, 3 H), 5.10 (s, 2 H), 4.81–4.93 (m, 1 H), 3.87 (overlapping s, 6 H), 3.13–3.28 (m, 2 H), 1.80–2.00 (m, 2 H), 1.42–1.59 (m, 2 H). MS (ES⁺) 455 (M + 1). HPLC: Kromasil C18 column (50 mm × 2 mm; 3.5 μ), gradient 10–90% (MeCN + 0.16% TFA) in (water + 0.2% TFA) over 4 min, *t*_R = 3.82 min (96%). A 500 mL hydrogenation vessel was charge with this material (19.49 g, 0.043 mol), ethyl acetate (80 mL), ethanol (70 mL), 1 N HCl (20 mL), and 10% palladium on carbon (2.0 g). The mixture was hydrogenated at 50 psig of hydrogen for 24 h, filtered through celite, and concentrated in vacuo to give 13.77 g (90%) of *N*-[4-amino-1-(*R*)-(3,4-dimethoxyphenyl)butyl]-2,2,2-trifluoroacetamide as a white solid. ¹H NMR δ 7.29–7.33 (m, 5 H), 6.81–6.86 (m, 3 H), 5.07 (s, 2 H), 4.80–4.89 (m, 1 H), 3.86 (overlapping s, 6 H), 3.15–3.25 (m, 2 H), 1.35–1.64 (m, 6 H). MS (ES⁺) 321 (M + 1). A 500 mL round-bottom flask containing this material (16.85 g, 0.047 mol), CH₂Cl₂ (220 mL), and triethylamine (14.0 mL, 0.10 mol) was cooled using an ice–water bath. Di-*tert*-butyl dicarbonate (9.77 g, 0.045 mol) was added in one portion. The mixture was stirred at room temperature for 18 h, diluted with CH₂Cl₂ (300 mL), and washed with 1 N HCl (1 × 100 mL), 1 N NaOH (1 × 100 mL), and water (1 × 100 mL). The organic layer was dried (MgSO₄), filtered through celite, and concentrated in vacuo to give 12.78 g (64%) of [4-(3,4-dimethoxyphenyl)-4-(*R*)-(2,2,2-trifluoroacetyl-amino)butyl]carbamic acid *tert*-butyl ester as a white solid. ¹H NMR δ 6.81–6.85 (m, 2 H), 6.78 (s, 1 H), 4.86–4.94 (m, 1 H), 3.89 (s, 3 H), 3.87 (s, 1 H), 3.09–3.24 (m, 2 H), 1.82–2.00 (m, 2 H), 1.47–1.57 (m, 2 H), 1.44 (s, 9 H). HPLC: Kromasil C18 column (50 mm × 2 mm; 3.5 μ), gradient 10–90% (MeCN + 0.16% TFA) in (water + 0.2% TFA) over 4 min, *t*_R = 3.95 min (99%). A 500 mL round-bottom flask was charged with [4-(3,4-dimethoxyphenyl)-4-(*R*)-(2,2,2-trifluoroacetyl-amino)butyl]carbamic acid *tert*-butyl ester (12.78 g, 0.030 mol), tetrahydrofuran (150 mL), methanol (40 mL), and 3 N NaOH (30 mL). After 3 h, the mixture was diluted with CH₂Cl₂ (500 mL) and washed with water (1 × 100 mL). The organic layer was dried with MgSO₄, filtered through celite, and concentrated in vacuo. The crude material was purified via flash silica gel chromatography (230–400 mesh silica gel 60, gradient 90:10–40:60 hexanes:ethyl acetate) to give 9.73 g (99%) of **XVI** as a white solid. ¹H NMR δ 6.87 (s, 1 H), 6.82–6.84 (m, 2 H), 3.84–3.90 (m, 7 H), 3.08–3.14 (m, 2 H), 1.62–1.71 (m, 4 H), 1.43 (s, 9 H). MS (ES⁺) 325 (M + 1). HPLC: Kromasil C18

column (50 mm \times 2 mm; 3.5 μ), gradient 10–90% (MeCN + 0.16% TFA) in (water + 0.2% TFA) over 4 min, t_R = 3.40 min (98%).

Synthesis of *N*-(2-Thiophenesulfonyl)-{4-(3,4-dimethoxyphenyl)-4-[4-(4-ethylpiperazin-1-yl)-1-oxo-2,3-dihydro-1*H*-isoindol-2-yl]butyl}amide (7a). 3-Bromo-2-methylbenzoic acid (15.3 g, 71 mmol) was dissolved in methanol (75 mL) and CH_2Cl_2 (425 mL), cooled to -5°C , and treated with 2 M trimethylsilyldiazomethane in hexanes (100 mL, 200 mmol) dropwise from an addition funnel. One hour after the addition of reagent, the reaction was complete by LC/MS. Evaporation of volatiles afforded methyl 3-bromo-2-methylbenzoate (16.6 g) as an oil. ^1H NMR δ 7.71 (t, J = 8 Hz, 2 H), 7.10 (d, J = 8 Hz, 1 H), 3.90 (s, 3 H), 2.63 (s, 3 H). HPLC: Kromasil C18 column (50 mm \times 2 mm; 3.5 μ), gradient 10–90% (MeCN + 0.16% TFA) in (water + 0.2% TFA) over 4 min, t_R = 4.25 (98%). This ester (16.6 g, 71 mmol), *N*-bromosuccinimide (13.09 g, 74 mmol), and benzoyl peroxide (0.56 g, 2.3 mmol) were dissolved in carbon tetrachloride (180 mL) and heated at 82°C (bath) overnight. The reaction was cooled to 23°C , diluted with ethyl acetate (600 mL), washed with water (300 mL), dried (MgSO_4), filtered, and concentrated in vacuo to afford **XVIII** as a solid (20.7 g, 95%), which was stored under argon in a freezer. ^1H NMR δ 7.89 (dd, J = 7.8 and 1.3 Hz, 1 H), 7.76 (dd, J = 8.0 and 1.3 Hz, 1 H), 7.23 (t, J = 8.0 Hz, 1 H), 5.13 (s, 2 H), 3.96 (s, 3 H). HPLC: Kromasil C18 column (50 mm \times 2 mm; 3.5 μ), gradient 10–90% (MeCN + 0.16% TFA) in (water + 0.2% TFA) over 4 min, t_R = 4.16 min (99%). (R)-**XVI** (3.04 g, 8.5 mmol) and triethylamine (1.2 mL, 8.6 mmol) were combined in toluene (50 mL) and treated with **XVIII** (2.4 g, 7.8 mmol) in toluene (100 mL) via an addition funnel. The reaction mixture was stirred at 23°C for 1 h, refluxed for 5 h, and evaporated. Purification on silica gel with an Analogix system (SF40–150 g, gradient elution with 0–2% methanol in CH_2Cl_2) afforded **XIX** (3.9 g, 82%) as a solid. ^1H NMR δ 7.79 (d, J = 8.0 Hz, 1 H), 7.39–7.49 (m, 2 H), 6.84–6.98 (m, 3 H), 5.53 (t, J = 7.9 Hz, 1 H), 4.26 and 3.96 (pair of d, J = 17 Hz, 1 H each), 3.87 (s, 3 H), 3.85 (s, 3 H), 3.18–3.25 (m, 2 H), 2.08–2.16 (m, 2 H), 1.50–1.60 (m, 2 H), 1.42 (s, 9 H). LC/MS (ES+) m/z 520 (M + 1). HPLC: Kromasil C18 column (50 mm \times 2 mm; 3.5 μ), gradient 10–90% (MeCN + 0.16% TFA) in (water + 0.2% TFA) over 4 min, t_R = 4.07 min (97%). Compound **XIX** (3.30 g, 6.0 mmol) was suspended in dry toluene (20 mL) under argon and treated with bis-(tri-*tert*-butylphosphine)palladium(0) (307 mg, 0.60 mmol), cetyl trimethylammonium bromide (120 mg, 0.33 mmol), and *N*-ethylpiperazine (2.75 g, 24 mmol). After adding 45% aqueous KOH solution (1.12 g, 9 mmol), the reaction mixture was purged well with argon, sealed with a Teflon screw cap, and heated to 105°C (bath) for 2 h. Analysis by LC/MS indicated 50% **XX** and 33% des-bromo compound. The reaction mixture was cooled to 23°C , decanted from solids, washed with additional toluene (25 mL), and evaporated in vacuo to afford a brown oil, which was dissolved in CH_2Cl_2 (200 mL), washed with saturated sodium bicarbonate (50 mL), water (50 mL), and brine (50 mL), dried (Na_2SO_4), and concentrated in vacuo to obtain a solid. The solid was dissolved in ethyl acetate, treated with silica gel (10 g), evaporated, and loaded onto a prepared column of silica gel (2 in. diameter, 200 g, 40:4:0.5 ethyl acetate/methanol/ammonium hydroxide) and eluted with the same. The product-containing fractions were evaporated, dissolved in ethyl acetate, dried (Na_2SO_4), and evaporated to give **XX** as a foamy solid (1.46 g, 44%). ^1H NMR δ 7.51 (d, J = 7.1 Hz, 1 H), 7.37–7.43 (m, 1 H), 7.08 (d, J = 7.4 Hz, 1 H), 6.82–6.96 (m, 3 H), 5.53 (t, J = 7.8 Hz, 1 H), 4.22 and 3.92 (pair of d, J = 17 Hz, 1 H each), 3.87 (s, 3 H), 3.84 (s, 3 H), 3.18–3.24 (m, 2 H), 3.05–3.12 (m, 4 H), 2.52–2.61 (m, 4 H), 2.05–2.15 (m, 2 H), 1.51–1.63 (m, 2 H), 1.42 (s, 9 H). LC/MS (ES+) m/z 553 (M + 1). HPLC: Kromasil C18 column (50 mm \times 2 mm; 3.5 μ), gradient 10–90% (MeCN + 0.16% TFA) in (water + 0.2% TFA) over 4 min, t_R = 3.15 min (96%). A 50 mL round-bottom flask was charged with **XX** (1.63

g, 2.95 mmol) and 1,4-dioxane (15.0 mL). A solution of 4 N HCl in 1,4-dioxane (10 mL) was added, and the mixture was stirred at 23°C for 4 h. The mixture was concentrated in vacuo to give solid (770 mg, 1.7 mmol), which was dissolved in CH_2Cl_2 (9 mL), cooled to 5°C , and treated with triethylamine (0.8 mL, 6 mmol) and 2-thiophenesulfonyl chloride (365 mg, 2.0 mmol) for 1 h. The reaction mixture was diluted with CH_2Cl_2 (200 mL), washed with 1 N HCl (50 mL), washed with saturated sodium bicarbonate (50 mL), dried (MgSO_4), and concentrated in vacuo to give an oil that was dissolved in CH_2Cl_2 (20 mL), treated with 1 N anhydrous HCl in diethyl ether, and concentrated in vacuo overnight to afford **7a** as a solid HCl salt (0.90 g, 88%). ^1H NMR δ 7.40–7.57 (m, 3 H), 7.37 (t, J = 7 Hz, 1 H), 7.06 (d, J = 8 Hz, 1 H), 7.00 (t, J = 4 Hz, 1 H), 6.80–6.92 (m, 3 H), 5.68 (broad s, 1 H, NH), 5.49 (t, J = 8 Hz, 1 H), 4.22 and 3.90 (pair of d, J = 17 Hz, 1 H each), 3.86 (s, 3 H), 3.82 (s, 3 H), 3.0 (m, 6 H), 2.61 (m, 4 H), 2.50 (m, 2 H), 2.16 (q, J = 7 Hz, 2 H), 1.59 (m, 2 H), 1.12 (t, J = 7 Hz, 3 H). LC/MS (ES+) m/z 599 (M + 1). Anal. calcd for $\text{C}_{30}\text{H}_{38}\text{N}_4\text{O}_5\text{S}_2 \cdot 1.8\text{HCl} \cdot 0.5\text{H}_2\text{O}$: C, 53.51; H, 6.11; N, 8.32; Cl, 9.48; H_2O , 1.34%. Found: C, 53.27; H, 6.04; N, 7.95; Cl, 9.44; H_2O , 1.46%. Compound **7a** was determined to be 96% ee [Daicel Chiralpak AD-H 25 cm \times 0.46 cm, heptane:2-propanol: Et_2NH (70:30:0.1), 0.7 mL/min, t_R = 20.6 min; its enantiomer had t_R = 12.2 min].

***N*-(2-Thiophenecarbonyl)-{4-(3,4-dimethoxyphenyl)-4-[4-(4-ethylpiperazin-1-yl)-1-oxo-2,3-dihydro-1*H*-isoindol-2-yl]butyl}amide (7c).** The crude BOC-deprotected solid (30 mg, 0.044 mmol) mentioned above (from **XX** in preparation of **7a**) was dissolved in DMF (2 mL) under nitrogen and treated with *N*-methylmorpholine (0.022 mL, 0.20 mmol), 1-methylimidazole-2-carboxylic acid (10 mg, 0.079 mmol), 1-hydroxybenzotriazole (HOBt; 4 mg, 0.03 mmol), *O*-benzotriazol-1-yl-*N,N,N'*-tetramethyluronium (HBTU) hexafluorophosphate (30 mg, 0.079 mmol) at 23°C overnight. The reaction mixture was diluted with water (4 mL) and acetonitrile (3 mL), filtered, and purified by reversed-phase HPLC [Phenomenex, Kromasil C18, 5 μ , 100 Å, 100 mm \times 21 mm, gradient elution with 10–50% acetonitrile (0.16% TFA) in water (0.2% TFA)] to yield **7c** (39 mg, quantitative). ^1H NMR δ 7.36–7.59 (m, 4 H), 6.81–7.09 (m, 5 H), 5.46–5.51 (m, 1 H), 4.22 and 3.88 (pair of d, J = 17.9 and 17 Hz, 1 H each), 3.87 (s, 3 H), 3.84 (s, 3 H), 3.49–3.60 (m, 4 H), 3.21–3.37 (m, 5 H), 2.97–3.12 (m, 2 H), 2.17–2.28 (m, 2 H), 1.72–1.85 (m, 2 H), 1.52–1.58 (m, 3 H). MS (ES+) 563 (M + 1). Anal. calcd for $\text{C}_{31}\text{H}_{38}\text{N}_4\text{O}_6\text{S} \cdot 2.1\text{HCl} \cdot 1.0\text{H}_2\text{O}$: C, 56.65; H, 6.46; N, 8.52; Cl, 11.33; H_2O , 2.74. Found: C, 56.30; H, 6.45; N, 8.34; Cl, 11.22; H_2O , 2.57.

Calcium Flux Assay. A calcium mobilization assay based on a Fluorescence Imaging Plate Reader (FLIPR; Molecular Devices, Sunnyvale, CA) was used to determine the agonist activity of the peptides in CHO cells transfected with rat GPR14 (U-II receptor).³⁹ To derive these cells, the complete coding sequence of rat U-II (Genbank Accession no. U32673) was amplified by nested PCR from rat heart marathon-ready cDNA. PCR was carried out by using the DNA polymerase PFU (Stratagene) following conditions suggested by the manufacturer. The PCR products were cloned into pcDNA3 (Invitrogen) digested with EcoR I and Xba I. Clones containing rat UT were verified by complete sequencing of the U-II receptor insert to ensure a lack of PCR-introduced errors. The constructed vector was transfected into CHO cells by using lipofectamine (GIBCO BRL). CHO cells with high expression of rat UT (determined by response to U-II in FLIPR-based calcium mobilization) were selected and established as stable cell lines by using G418. CHO cells were seeded at 40000 cells per well into 96-well, black-wall, clear-bottom microtiter plates 24 h before running the assay. Cells in culture media (DMEM/F12 containing 15 mM HEPES, L-glutamine, pyridoxine hydrochloride, 10% fetal bovine serum, 1 mg/mL G418 sulfate, antibiotic/antimycotic, pH 7.4) were loaded with proprietary dye, from the FLIPR calcium assay kit (Molecular Devices),

prepared in assay buffer (Hanks Balanced Salts Solution, 20 mM HEPES, 0.1% bovine serum albumin (BSA), 2.5 mM probenecid, pH 7.4), and incubated for 1 h at 37 °C. Calcium mobilization determinations were performed at 23 °C. EC₅₀ values were calculated relative to the maximum calcium ionophore (A23187) response at 10 μM. Antagonist activity of inactive compounds was assessed, after a 10 min of incubation, in response to an agonist, such as goby U-II (0.1 nM) or peptide **1** (0.3 or 1 nM). The use of rat GPR14 and the goby peptide was considered acceptable because human and goby U-II have similar affinity for human or rat GPR14 in the transfected cells.⁶

Radioligand Binding Assay.²⁴ CHO cells stably expressing rat GPR14³⁹ (UT) were harvested and washed with ice-cold phosphate buffered saline (PBS, pH 7.4) and resuspended in 20 mM Tris-HCl (pH 7.4), 250 mM sucrose, and 1 mM ethyleneglycol tetraacetic acid. Cells were homogenized in a glass–Teflon homogenizer and, after centrifugation at 1000g for 15 min, the resulting supernatant was obtained and recentrifuged at 30000g for 60 min at 4 °C. The resulting pellet was passed through a 25 gauge needle five times, and membranes were stored at –80 °C. Membranes were precoupled to wheat germ agglutinin-coated scintillation-proximity assay (SPA) beads (Amersham Pharmacia Biotech, England, UK) at the concentration of 15 μg membrane/mg beads. The coupling was carried out for 30 min at room temperature in buffer A (50 mM Tris-HCl, 5 mM MgCl₂, and 0.1% BSA adjusted to pH 7.4) with continual shaking. After a brief spin, the supernatant was discarded. The assay was conducted in 96-well microtiter plates, with a final concentration of 1.0 mg of precoupled beads per well, 0.17 nM moniodinated [¹²⁵I]-[Tyr]-rat U-II (Phoenix Pharmaceuticals, Belmont, CA), and various concentrations of compounds in a total volume of 100 μL buffer A. The plate was shaken for 3 h at 22 °C, and after a brief spin, the radioactivity was counted by using a Topcount instrument (Packard Bioscience Company, Meriden, CT). Nonspecific binding, determined using 1 μM rat U-II, was always less than 15% of the total binding. The GraphPad Prism software package (GraphPad Software, Inc., San Diego, CA) was used to analyze the binding data, and K_i values were calculated (*n* = 2) by the Cheng–Prusoff equation.

Functional Assay in Rat Aortic Rings.²⁷ Selected compounds were tested for contractile effects on rat thoracic aorta smooth muscle at a concentration of 30 nM. The response (*n* = 2) was measured relative to that produced by 80 mM KCl. These studies were conducted by CEREP (Celle L'Evescault, France). The aortas were obtained from male Wistar rats (250 g; CERJ, Le Genest St. Isle, France). The animals were sacrificed by cervical dislocation followed by exsanguination, and the aortas were quickly removed, cleaned, and dissected into rings. The rings were suspended between two stainless steel hooks in organ baths containing 20 mL of an oxygenated and prewarmed physiological salt solution. They were connected to force-displacement transducers (UF1, Phymep) for isometric tension recordings. Data were continuously recorded on a multichannel data acquisition system. The physiological salt solution contained the following (mM): NaCl, 118.0; KCl, 4.7; MgSO₄, 1.2; CaCl₂, 2.5; KH₂PO₄, 1.2; NaHCO₃, 25.0; glucose, 11.0. The high-K⁺ (80 mM) solutions were prepared by equimolar replacement of NaCl with KCl. These solutions were continuously aerated with a 95% O₂/5% CO₂ gas mixture and maintained at pH 7.4 and 37 °C. Goby U-II (Palomar Research, Inc., cat. no. U4832, lot no. A34001-298M) and test compounds were freshly prepared in stock solutions by using physiological buffer. The aortic rings were stretched to an optimal resting tension and then allowed to equilibrate for at least 30 min, during which time they were washed repeatedly. Each ring was contracted using a high KCl solution (80 mM) to verify responsiveness and to obtain a maximal contractile response. The rings were again washed until resting tension returned to baseline and then they were exposed to 30 nM of the test compound

(*n* = 2/test compound) until a stable response was obtained or for a maximum of 30 min. The degree of contraction was expressed as a percentage of the KCl-induced maximal contraction.

Acknowledgment. We thank Benoit Liégault for initial development of the palladium-catalyzed aryl amination reaction and Andrew Mahan for chiral HPLC analyses.

Supporting Information Available: Characterization data for compounds **2**, (*R*)-**4**, (*S*)-**4**, **5a–g**, **5k–m**, (*R,R*)-**5a**, (*R*)-**5j**, (*S*)-**5j**, **6a–j**, **7b**, **7d–o**. Energy-minimized structures for **7a** and **8–12**. This material is available free of charge via the Internet at <http://pubs.acs.org>.

References

- (1) For reviews, see: (a) Onan, D.; Hannan, R. D.; Thomas, W. G. Urotensin II: the old kid in town. *Trends Endocrinol. Metab.* **2004**, *15*, 175–182. (b) Doggrel, S. A. Urotensin-II and the cardiovascular system—the importance of developing modulators. *Expert Opin. Investig. Drugs* **2004**, *13*, 479–487. (c) Douglas, S. A.; Dhanak, D.; Johns, D. G. From “gills to pills”: urotensin-II as a regulator of mammalian cardiorenal function. *Trends Pharmacol. Sci.* **2004**, *25*, 76–85. (d) Ong, K. L.; Lam, K. S. L.; Cheung, B. M. Y. Urotensin II: its function in health and its role in disease. *Cardiovasc. Drugs Ther.* **2005**, *19*, 65–75. (e) Carmine, Z.; Mallamaci, F. Urotensin II: a cardiovascular and renal update. *Curr. Opin. Nephrol. Hypertens.* **2008**, *17*, 199–204. (f) Proulx, C. D.; Holleran, B. J.; Lavigne, P.; Escher, E.; Guillemette, G.; Leduc, R. Biological properties and functional determinants of the urotensin II receptor. *Peptides* **2008**, *29*, 691–699. (g) Maryanoff, B. E.; Kinney, W. A. Urotensin-II receptor modulators as potential drugs. *J. Med. Chem.*, in press.
- (2) (a) Pearson, D.; Shively, J. E.; Clark, B. R.; Geschwind, I. I.; Barkley, M.; Nishioka, R. S.; Bern, H. A. Urotensin II: A somatostatin-like peptide in the caudal neurosecretory system of fishes. *Proc. Natl. Acad. Sci. U.S.A.* **1980**, *77*, 5021–5024. (b) Coulouarn, Y.; Lihmann, I.; Jegou, S.; Anouar, Y.; Tostivint, H.; Beauvillain, J. C.; Conlon, J. M.; Bern, H. A.; Vaudry, H. Cloning of the cDNA encoding the urotensin II precursor in frog and human reveals intense expression of the urotensin II gene in motoneurons of the spinal cord. *Proc. Natl. Acad. Sci. U.S.A.* **1998**, *95*, 15803–15808. (c) Ames, R. S.; Sarau, H. M.; Chambers, J. K.; Willette, R. N.; Aiyar, N. V.; Romanic, A. M.; Loudon, C. S.; Foley, J. J.; Sauermelch, C. F.; Coatney, R. W.; Ao, Z.; Disa, J.; Holmes, S. D.; Stadel, J. M.; Martin, J. D.; Liu, W.-S.; Glover, G. I.; Wilson, S.; McNulty, D. E.; Ellis, C. E.; Elshourbagy, N. A.; Shabon, U.; Trill, J. J.; Hay, D. W. P.; Ohlstein, E. H.; Bergsma, D. J.; Douglas, S. A. Human urotensin-II is a potent vasoconstrictor and agonist for the orphan receptor GPR14. *Nature* **1999**, *401*, 282–286. (d) Elshourbagy, N. A.; Douglas, S. A.; Shabon, U.; Harrison, S.; Duddy, G.; Sechler, J. L.; Ao, Z.; Maleeff, B. E.; Naselsky, D.; Disa, J.; Aiyar, N. V. Molecular and pharmacological characterization of genes encoding urotensin-II peptides and their cognate G-protein-coupled receptors from the mouse and monkey. *Br. J. Pharmacol.* **2002**, *136*, 9–22. (e) Maguire, J. J.; Kuc, R. E.; Kleinz, M. J.; Davenport, A. P. Immunocytochemical localization of the urotensin-II receptor, UT, to rat and human tissues: relevance to function. *Peptides* **2008**, *29*, 735–742.
- (3) (a) Flohr, S.; Kurz, M.; Kostenis, E.; Brkovich, A.; Fournier, A.; Klabunde, T. Identification of nonpeptidic urotensin II receptor antagonists by virtual screening based on a pharmacophore model derived from structure–activity relationships and nuclear magnetic resonance studies on urotensin II. *J. Med. Chem.* **2002**, *45*, 1799–1805. (b) Kinney, W. A.; Almond, H. R., Jr.; Qi, J.; Smith, C. E.; Santulli, R. J.; de Garavilla, L.; Andrade-Gordon, P.; Cho, D. S.; Everson, A. M.; Feinstein, M. A.; Leung, P. A.; Maryanoff, B. E. Structure–function analysis of urotensin II and its use in the construction of a ligand–receptor working model. *Angew. Chem., Int. Ed.* **2002**, *41*, 2940–2944. (c) Brkovic, A.; Hattenberger, A.; Kostenis, E.; Klabunde, T.; Flohr, S.; Kurz, M.; Bourgault, S.; Fournier, A. Functional and binding characterizations of urotensin II-related peptides in human and rat urotensin II-receptor assay. *J. Pharmacol. Exp. Ther.* **2003**, *306*, 1200–1209.
- (4) Conlon, J. M.; Yano, K.; Waugh, D.; Hazon, N. Distribution and molecular forms of urotensin II and its role in cardiovascular regulation in vertebrates. *J. Exp. Zool.* **1996**, *275*, 226–238.
- (5) Bohm, F.; Pernow, J. Urotensin II evokes potent vasoconstriction in humans in vivo. *Br. J. Pharmacol.* **2002**, *135*, 25–27.
- (6) Douglas, S. A.; Ohlstein, E. H. Human urotensin-II, the most potent mammalian vasoconstrictor identified to date, as a therapeutic target for the management of cardiovascular disease. *Trends Cardiovasc. Med.* **2000**, *10*, 229–237.

- (7) Gardiner, S. M.; March, J. E.; Kemp, P. A.; Davenport, A. P.; Bennett, T. Depressor and regionally-selective vasodilator effects of human and rat urotensin II in conscious rats. *Br. J. Pharmacol.* **2001**, *132*, 1625–1629.
- (8) Zou, Y.; Nagai, R.; Yamazaki, T. Urotensin II induces hypertrophic responses in cultured cardiomyocytes from neonatal rats. *FEBS Lett.* **2001**, *508*, 57–60.
- (9) Watanabe, T.; Pakala, R.; Katagiri, T.; Benedict, C. R. Synergistic effect of urotensin II with mildly oxidized LDL on DNA synthesis in vascular smooth muscle cells. *Circulation* **2001**, *104*, 16–18.
- (10) (a) Matsushita, M.; Shichiri, M.; Imai, T.; Iwashina, M.; Tanaka, H.; Takasu, N.; Hirata, Y. Co-expression of urotensin II and its receptor (GPR14) in human cardiovascular and renal tissues. *J. Hypertens.* **2001**, *19*, 2185–2190. (b) Krum, H.; Kemp, W. Therapeutic potential of blockade of the urotensin II system in systemic hypertension. *Curr. Hypertens. Rep.* **2007**, *9*, 53–58.
- (11) (a) Douglas, S. A.; Tayara, L.; Ohlstein, E. H.; Halawa, N.; Giaid, A. Congestive heart failure and expression of myocardial urotensin II. *Lancet* **2002**, *359*, 1990–1997. (b) Tzanidis, A.; Hannan, R. D.; Thomas, W. G.; Onan, D. J.; See, F.; Kelly, D. J.; Gilbert, R. E.; Krum, H. Direct actions of urotensin II on the heart. Implications for cardiac fibrosis and hypertrophy. *Circ. Res.* **2003**, *93*, 246–253. (c) Tolle, M.; van der Giet, M. Cardioresvascular effects of urotensin II and the relevance of the UT receptor. *Peptides* **2008**, *29*, 743–763.
- (12) (a) Totsune, K.; Takahashi, K.; Arihara, Z.; Sone, M.; Satoh, F.; Ito, S.; Kimura, Y.; Sasano, H.; Murakami, O. Role of urotensin II in patients on dialysis. *Lancet* **2001**, *358*, 810–811. (b) Langham, R. G.; Kelly, D. J.; Gow, R. M.; Zhang, Y.; Dowling, J. K.; Thomson, N. M.; Gilbert, R. E. Increased expression of urotensin II and urotensin II receptor in human diabetic nephropathy. *Am. J. Kidney Dis.* **2004**, *44*, 826–831.
- (13) (a) Totsune, K.; Takahashi, K.; Arihara, Z.; Sone, M.; Ito, S.; Murakami, O. Increased plasma urotensin II levels in patients with diabetes mellitus. *Clin. Sci.* **2003**, *104*, 1–5. (b) Wenyi, Z.; Suzuki, S.; Hirai, M.; Hinokio, Y.; Tanizawa, Y.; Matsutani, A.; Satoh, J.; Oka, Y. Role of urotensin II gene in genetic susceptibility to Type 2 diabetes mellitus in Japanese subjects. *Diabetologia* **2003**, *46*, 972–976. (c) Ong, K. L.; Wong, L. Y. F.; Cheung, B. M. Y. The role of urotensin II in the metabolic syndrome. *Peptides* **2008**, *29*, 859–867.
- (14) (a) Watanabe, T.; Kanome, T.; Suguro, T.; Miyazaki, A. Human urotensin II and metabolic syndrome. *Vasc. Dis. Prev.* **2006**, *3*, 91–98. (b) Bousette, N.; Patel, L.; Douglas, S. A.; Ohlstein, E. H.; Giaid, A. Increased expression of urotensin II and its cognate receptor GPR14 in atherosclerotic lesions of the human aorta. *Atherosclerosis* **2004**, *176*, 117–123. (c) Loirand, G.; Rolli-Derkinderen, M.; Pacaud, P. Urotensin II and atherosclerosis. *Peptides* **2008**, *29*, 778–782.
- (15) Luci, D. K.; Ghosh, S.; Smith, C. E.; Qi, J.; Wang, Y.; Haertlein, B.; Parry, T. J.; Li, J.; Almond, H. R.; Minor, L. K.; Damiano, B. P.; Kinney, W. A.; Maryanoff, B. E.; Lawson, E. C. Phenylpiperidine-benzoxazinones as urotensin-II receptor antagonists: synthesis, SAR, and in vivo assessment. *Bioorg. Med. Chem. Lett.* **2007**, *17*, 6489–6492.
- (16) For reviews, see: (a) Jin, J.; Douglas, S. A. Non-peptidic urotensin-II receptor modulators. *Expert Opin. Ther. Pat.* **2006**, *16*, 467–479. (b) Carotenuto, A.; Grieco, P.; Rovero, P.; Novellino, E. Urotensin-II receptor antagonists. *Curr. Med. Chem.* **2006**, *13*, 267–275. (c) Lescot, E.; Bureau, R.; Rault, S. Nonpeptide urotensin-II receptor agonists and antagonists: review and structure–activity relationships. *Peptides* **2008**, *29*, 680–690.
- (17) (a) Jin, J.; Wang, Y.; Wang, F.; Shi, D.; Erhard, K. F.; Wu, Z.; Guida, B. F.; Lawrence, S. K.; Behm, D. J.; Disa, J.; Vaidya, K. S.; Evans, C.; McMillan, L. J.; Rivero, R. A.; Neeb, M. J.; Douglas, S. A. 2-Aminomethyl piperidines as novel urotensin-II receptor antagonists. *Bioorg. Med. Chem. Lett.* **2008**, *18*, 2860–2864. (b) Jin, J.; Dhanak, D.; Knight, S. D.; Widdowson, K.; Aiyar, N.; Naselsky, D.; Sarau, H. M.; Foley, J. J.; Schmidt, D. B.; Bennett, C. D.; Wang, B.; Warren, G. L.; Moore, M. L.; Keenan, R. M.; Rivero, R. A.; Douglas, S. A. Aminoalkoxybenzyl pyrrolidines as novel human urotensin-II receptor antagonists. *Bioorg. Med. Chem. Lett.* **2005**, *15*, 3229–3232. (c) Clozel, M.; Hess, P.; Qiu, C.; Ding, S. S.; Rey, M. The urotensin-II receptor antagonist palosuran improves pancreatic and renal function in diabetic rats. *J. Pharmacol. Exp. Ther.* **2006**, *316*, 1115–1121. (d) McAtee, J. J.; Dodson, J. W.; Dowdell, S. E.; Girard, G. R.; Goodman, K. B.; Hilfiker, M. A.; Sehon, C. A.; Sha, D.; Wang, G. Z.; Wang, N.; Viet, A. Q.; Zhang, D.; Aiyar, N. V.; Behm, D. J.; Carballo, L. H.; Evans, C. A.; Fries, H. E.; Nagilla, R.; Roethke, T. J.; Xu, X.; Yuan, C. C. K.; Douglas, S. A.; Neeb, M. J. Development of potent and selective small-molecule human urotensin-II antagonists. *Bioorg. Med. Chem. Lett.* **2008**, *18*, 3500–3503. (e) McAtee, J. J.; Dodson, J. W.; Dowdell, S. E.; Erhard, K.; Girard, G. R.; Goodman, K. B.; Hilfiker, M. A.; Jin, J.; Sehon, C. A.; Sha, D.; Shi, D.; Wang, F.; Wang, G. Z.; Wang, N.; Wang, Y.; Viet, A. Q.; Yuan, C. C. K.; Zhang, D.; Aiyar, N. V.; Behm, D. J.; Carballo, L. H.; Evans, C. A.; Fries, H. E.; Nagilla, R.; Roethke, T. J.; Xu, X.; Yuan, C. C. K.; Douglas, S. A.; Neeb, M. J. Potent and selective small-molecule human urotensin-II antagonists with improved pharmacokinetic profiles. *Bioorg. Med. Chem. Lett.* **2008**, *18*, 3716–3719. (f) Jin, J.; An, M.; Sapienza, A.; Aiyar, N.; Naselsky, D.; Sarau, H. M.; Foley, J. J.; Salyers, K. L.; Knight, S. D.; Keenan, R. M.; Rivero, R. A.; Dhanak, D.; Douglas, S. A. Urotensin-II receptor antagonists: Synthesis and SAR of N-cyclic azaalkyl benzamides. *Bioorg. Med. Chem. Lett.* **2008**, *18*, 3950–3954. (g) Hilfiker, M. A.; Zhang, D.; Dowdell, S. E.; Goodman, K. B.; McAtee, J. J.; Dodson, J. W.; Viet, A. Q.; Wang, G. Z.; Sehon, C. A.; Behm, D. J.; Wu, Z.; Carballo, L. H.; Douglas, S. A.; Neeb, M. J. Aminomethylpiperazines as selective urotensin antagonists. *Bioorg. Med. Chem. Lett.* **2008**, *18*, 4470–4473. (h) Wang, Y.; Wu, Z.; Guida, B. F.; Lawrence, S. K.; Neeb, M. J.; Rivero, R. A.; Douglas, S. A.; Jin, J. N-Alkyl-5H-pyrido[4,3-b]indol-1-amine and derivatives as novel urotensin-II receptor antagonists. *Bioorg. Med. Chem. Lett.* **2008**, *18*, 4936–4939. (i) Clozel, M.; Binkert, C.; Birker-Robaczewska, M.; Boukhadra, C.; Ding, S.-S.; Fischli, W.; Hess, P.; Mathys, B.; Morrison, K.; Mueller, C.; Mueller, C.; Nayler, O.; Qiu, C.; Rey, M.; Scherz, M. W.; Velker, J.; Weller, T.; Xi, J.-F.; Ziltener, P. Pharmacology of the urotensin-II receptor antagonist palosuran (ACT-058362; 1-[2-(4-benzyl-4-hydroxypiperidin-1-yl)-ethyl]-3-(2-methylquinolin-4-yl)urea sulfate salt): first demonstration of a pathophysiological role of the urotensin system. *J. Pharmacol. Exp. Ther.* **2004**, *311*, 204–212.
- (18) Nahm, S.; Weinreb, S. M. N-Methoxy-N-methylamides as effective acylating agents. *Tetrahedron Lett.* **1981**, *22*, 3815–3818.
- (19) Ponzio, V. L.; Kaufman, T. S. A simple protocol for the one pot synthesis of chiral secondary benzylic alcohols by catalytic enantioselective reduction of aromatic ketones. *Synlett* **2002**, *7*, 1128–1130.
- (20) Garro-Helion, F.; Merzouk, A.; Guibe, F. Mild and selective palladium(0)-catalyzed deallylation of allylic amines. Allylamine and diallylamine as very convenient ammonia equivalents for the synthesis of primary amines. *J. Org. Chem.* **1993**, *58*, 6109–6113.
- (21) (a) Kadyrov, R.; Riermeier, T. H. Highly enantioselective hydrogen-transfer reductive amination: catalytic asymmetric synthesis of primary amines. *Angew. Chem., Int. Ed.* **2003**, *42*, 5472–5474. (b) Each enantiomer of intermediate XV was analyzed by chiral HPLC (see Experimental Section).
- (22) Kuwano, R.; Utsunomiya, M.; Hartwig, J. F. Aqueous hydroxide as a base for palladium-catalyzed amination of aryl chlorides and bromides. *J. Org. Chem.* **2002**, *67*, 6479–6486.
- (23) (S)-**4** had an IC₅₀ value of 460 nM.
- (24) Qi, J.-S.; Minor, L. K.; Smith, C.; Hu, B.; Yang, J.; Andrade-Gordon, P.; Damiano, B. Characterization of functional urotensin II receptors in human skeletal muscle myoblasts: comparison with angiotensin II receptors. *Peptides* **2005**, *26*, 683–690.
- (25) There was virtually no difference in potency between (R,S)-**5a** and its diastereomer at the dimethoxybenzyl group, (R,R)-**5a** (IC₅₀ = 150 nM).
- (26) Douglas, S. A.; Behm, D. J.; Aiyar, N. V.; Naselsky, D.; Disa, J.; Brooks, D. P.; Ohlstein, E. H.; Gleason, J. G.; Sarau, H. M.; Foley, J. J.; Buckley, P. T.; Schmidt, D. B.; Wixted, W. E.; Widdowson, K.; Riley, G.; Jin, J.; Gallagher, T. F.; Schmidt, S. J.; Ridgers, L.; Christmann, L. T.; Keenan, R. M.; Knight, S. D.; Dhanak, D. Nonpeptidic urotensin-II receptor antagonists I: in vitro pharmacological characterization of SB-706375. *Br. J. Pharmacol.* **2005**, *145*, 620–635.
- (27) Herold, C. L.; Behm, D. J.; Buckley, P. T.; Foley, J. J.; Wixted, W. E.; Sarau, H. M.; Douglas, S. A. The neuromedin B receptor antagonist, BIM-23127, is a potent antagonist at human and rat urotensin-II receptors. *Br. J. Pharmacol.* **2003**, *139*, 203–207.
- (28) Qi, J.; Schulingkamp, R.; Parry, T. J.; Colburn, R.; Stone, D.; Haertlein, B.; Minor, L. K.; Andrade-Gordon, P.; Damiano, B. P. Urotensin-II induces ear flushing in rats. *Br. J. Pharmacol.* **2007**, *150*, 415–423.
- (29) Cerep (Seattle, WA; www.cerep.com), an independent contract laboratory, performed standardized binding assays on receptors and ion channels. Each results was expressed as percent inhibition of a control specific binding (mean values, n = 2; human).
- (30) Receptors and channels, < 50% inhibition at 10 μM: adenosine A1 (h), A2A (h), A3 (h); adrenergic α-2, β (h); angiotensin AT1 (h); central benzodiazepine; bradykinin B2 (h); cholecystinin CCK-A (h); dopamine D1 (h), D2S (h); endothelin ET-A (h); γ-aminobutyric acid (GABA); galanin GAL2 (h); CXCR2 (h); CCR1 (h); histamine H1 (h), H2 (h); melanocortin MC4 (h); melatonin MT1 (h); muscarinic M2; neukinin NK2 (h), NK3 (h); neuropeptide Y NPY1 (h), NPY2 (h); neurotensin NT1 (h); opioid δ2 (h), κ, μ (h); ORL1 (NOP) (h); serotonin 5HT2A (h), 5-HT3 (h), 5-HT-5A (h), 5-HT6 (h), 5-HT7 (h); somatostatin; vasoactive intestinal peptide VIP (h); vasopressin V1a (h); L, SK Ca²⁺ channels; K⁺ channel; Cl⁻ channel; norepinephrine transporter; dopamine transporter.

- (31) *Maestro 8.5.207*; Schrodinger, Inc.: 1500 SW First Avenue, Suite 1180, Portland, OR.
- (32) Jorgensen, W. L.; Tirado-Rives, J. The OPLS [optimized potentials for liquid simulations] potential functions for proteins, energy minimizations for crystals of cyclic peptides and crambin. *J. Am. Chem. Soc.* **1988**, *110*, 1657–1666.
- (33) Qui, D.; Shenkin, P. S.; Hollinger, F. P.; Still, C. W. The GB/SA continuum model for solvation. A fast analytical method for the calculation of approximate Born radii. *J. Phys. Chem. A* **1997**, *101*, 3005–3014.
- (34) (a) Kolossvary, I.; Guida, W. C. Low mode search. An efficient, automated computational method for conformational analysis: application to cyclic and acyclic alkanes and cyclic peptides. *J. Am. Chem. Soc.* **1996**, *118*, 5011–5019. (b) Kolossvary, I.; Guida, W. C. Low-mode conformational search elucidated: application to C₃₉H₈₀ and flexible docking of 9-deazaguanine inhibitors into PNP. *J. Comput. Chem.* **1999**, *20*, 1671–1684.
- (35) *Phase, Version 3.0*; Schrodinger, LLC: New York, 2008.
- (36) Luci, D. K.; Lawson, E. C.; Ghosh, S.; Kinney, W. A.; Smith, C. E.; Qi, J.; Wang, Y.; Minor, L. K.; Maryanoff, B. E. Generation of novel, potent urotensin-II receptor antagonists by alkylation–cyclization of isoindolinone C3-carbanions. *Tetrahedron Lett.* **2009**, *50*, 4958–4961.
- (37) (a) Lescot, E.; Sopkova-de Oliveira Santos, J.; Dubessy, C.; Oulyadi, H.; Lesnard, A.; Vaudry, H.; Bureau, R.; Rault, S. Definition of new pharmacophores for nonpeptide antagonists of urotensin-II. Comparison with the 3D-structure of human urotensin-II and URP. *J. Chem. Inf. Model.* **2007**, *47*, 602–612. (b) Lescot, E.; Sopkova-de Oliveira Santos, J.; Colloc'h, N.; Rodrigo, J.; Milazzo-Segalas, I.; Bureau, R.; Rault, S. Three-dimensional model of the human urotensin-II receptor: docking of human urotensin-II and nonpeptide antagonists in the binding site and comparison with an antagonist pharmacophore model. *Proteins* **2008**, *73*, 173–184.
- (38) Kitamura, M.; Tokunaga, M.; Ohkuma, T.; Noyori, R. Asymmetric hydrogenation of 3-oxo carboxylates using BINAP-ruthenium complexes: (R)-(-)-methyl 3-hydroxybutanoate. *Org. Synth.* **1993**, *71*, 1–13.
- (39) (a) Tal, M.; Ammar, D. A.; Karpuj, M.; Krizhanovsky, V.; Naim, M.; Thompson, D. A. A novel putative neuropeptide receptor expressed in neural tissue, including sensory epithelia. *Biochem. Biophys. Res. Commun.* **1995**, *209*, 752–759. (b) Marchese, A.; Heiber, M.; Nguyen, T.; Heng, H. H.; Saldivia, V. R.; Cheng, R.; Murphy, P. M.; Tsui, L. C.; Shi, X.; Gregor, P. Cloning and chromosomal mapping of three novel genes, GPR9, GPR10, and GPR14, encoding receptors related to interleukin 8, neuropeptide Y, and somatostatin receptors. *Genomics* **1995**, *29*, 335–344.